



## Late Holocene cryptotephra from Cascade Lake, Alaska: supporting data for a 21,000-year multi-chronometer Bayesian age model

Lauren J. Davies<sup>1,2</sup>, Britta J. L. Jensen<sup>1</sup>, Darrell S. Kaufman<sup>3</sup>

5 <sup>1</sup>Department of Earth and Atmospheric Sciences, University of Alberta, Edmonton, AB,  
Canada

<sup>2</sup>Department of Geography, University of Cambridge, Cambridge, UK

<sup>3</sup>School of Earth and Sustainability, Northern Arizona University, Flagstaff, Arizona, USA

*Correspondence to:* Lauren J. Davies (ld636@cam.ac.uk)

10 **Abstract.** Multiple chronometers can be employed for dating Holocene  
palaeoenvironmental records, each with its own inherent strengths and weaknesses.  
Radiocarbon dating is one of the most widely used techniques for producing chronologies,  
but its application at high-latitude sites can be problematic. Here, cryptotephra identified in  
15 the Late Holocene portion of a core from Cascade Lake, Arctic Alaska, resolve a divergence  
identified between radiocarbon and paleomagnetic secular variation (PSV) data in the top 1.5  
m of the sediment sequence. Identifiable geochemical populations of cryptotephra are shown  
to be present in detectable concentrations in sediment from the north flank of the Brooks  
Range for the first time. Major element glass geochemical correlations are demonstrated  
20 between ultra-distal cryptotephra and reference samples from the Late Holocene caldera  
forming eruption of Opala, Kamchatka, as well as three eruptions in North America: the  
White River Ash (northern lobe), Ruppert tephra and the Late Holocene caldera forming  
eruption of Aniakchak. The correlated ages of these cryptotephra support the PSV ages  
reported in Steen et al. (this volume) and provide evidence for an old-carbon effect in  
25 Cascade Lake. Chronological data from the Cascade Lake were then combined using a  
Bayesian approach to generate an age-depth model that extends back to 21,000 cal yr BP.

### 1 Introduction

The accuracy and precision of ages and chronological models produced from  
sedimentary records directly impacts the utility and value of the associated proxies used for  
palaeoenvironmental reconstructions. In Arctic North America, the majority of Holocene to  
30 late Pleistocene palaeoenvironmental reconstructions are produced from lake and peat  
deposits (e.g. Kaufman et al., 2016), and often rely on radiocarbon (<sup>14</sup>C) dating to develop  
age models.

However, there are several issues that can affect the application and interpretation of  
<sup>14</sup>C ages in Arctic regions. Firstly, there may be a lack of organic material in lake sediment  
35 cores or the terrestrial macrofossils that are often preferred for dating (e.g. Oswald et al.,  
2005; Turney et al., 2000) may be absent. This can be a particular problem for sediments that  
accumulated during colder periods. Secondly, high-latitude regions often have an abundance



of old carbon due to slow rates of decomposition in cold, typically nutrient poor soils (e.g. Gaglioti et al., 2014; Schuur et al., 2008), erosion from the surrounding sediments or  
40 bedrock, and the reworking and redeposition of older, well-preserved macrofossils (e.g. Kennedy et al., 2010).

More broadly,  $^{14}\text{C}$  samples can also be affected by issues relating to sample selection, remobilisation, the hard-water effect and contamination (for a general review of these topics see, e.g. Olsson, 1974; Lowe and Walker, 2000). These factors can contribute to complicated  
45 resulting age models for Arctic sediments that require careful independent verification. For example, the use of bulk sediments for dating has been shown to incorporate organic fractions of varying ages (e.g. Brock et al., 2011; Nelson et al., 1988) and hard-water effects have long been known in North American lakes (e.g. Abbott and Stafford, 1996; Karrow and Anderson, 1975; Moore et al., 1998).

50 The combination of multiple chronometers has been successfully used to highlight differences between chronological methods and produce more accurate final age models for lacustrine and peat cores (Davies et al., 2018; Tylmann et al., 2016). Two additional techniques that have been applied in Arctic areas are discussed here - palaeomagnetic secular variation (PSV) and tephrochronology.

### 55 **1.1 Palaeomagnetic chronologies**

In recent years there have been an increasing number of studies looking to improve chronologies of late Quaternary Arctic sedimentary sequences by using palaeomagnetic data (e.g. Barletta et al., 2008; Deschamps et al., 2018; Lund et al., 2016; Ólafsdóttir et al., 2013). Sediments at high-latitude sites can be sensitive to palaeomagnetic secular variation (PSV) –  
60 small directional changes in the geomagnetic field (Cox, 1970) that are preserved in sediment through the alignment of magnetic mineral grains with Earth's ambient field around the time of deposition. Tie-points, identified using peaks and troughs, can then be dated and used as correlative chronostratigraphic tools. These ages can be produced from both individual site measurements and geomagnetic model calculations. PSV correlation techniques are useful as  
65 they can produce more frequent data points and be applied beyond the limits of  $^{14}\text{C}$  dating, or where organic material is not preserved. Their use, however, is limited geographically as high-latitude geomagnetic field dynamics are spatially complex (e.g. Stoner et al., 2013).

70 Steen et al. (this volume) report PSV-correlated ages for cores from Cascade Lake, Alaska, that have substantial offsets during the Late Holocene from  $^{14}\text{C}$  ages from the same sediment. Over the top 175 cm of the core,  $^{14}\text{C}$  ages are up to ~2000 years older than



palaeomagnetic correlated ages. When using multiple chronometers from the same sediment there is not always coherence or clear agreement between the results and additional chronological information is required. Here, a third chronostratigraphic technique – tephrochronology – was applied to Cascade Lake sediments to resolve the offset.

## 75 1.2 Cryptotephra chronologies

Cryptotephra - non-visible horizons of volcanic ash from distal sources – have been studied globally (see, e.g. Davies, 2015; Lowe et al., 2017) and are a useful chronostratigraphic tool (Pilcher et al., 1995; Plunkett, 2006; Swindles et al., 2010). Where correlations can be made with well-dated tephra (e.g. historical eruptions, or tephra preserved  
80 within annually resolved records), tightly constrained associated ages can be included in age-depth models (e.g. Schoning et al., 2005). They can also be used as an independent test of other chronological methods applied to the same record (e.g. Davies et al., 2018; Oldfield et al., 1997).

In Alaska and northern Canada the majority of tephra studies have been limited to  
85 areas where visible tephra are present and only a few studies have identified cryptotephra (e.g. de Fontaine et al., 2007; Lakeman et al., 2008; Monteath et al., 2017; Payne et al., 2008; Zoltai, 1989). However, there is significant potential for cryptotephra to be found in Alaska as it is downwind of a large number of volcanoes known to have been active over the Holocene. Of Alaska's 130 volcanoes and volcanic fields, 96 have been active either  
90 historically or within the Holocene (Miller et al., 1998) and historical observations show that more than 50 volcanoes have been active since ~ 1760 AD alone (Alaska Volcano Observatory, 2016). Here, key tephra are from historical eruptions, or eruptions that produced regionally widespread tephra within Alaska and have precise age estimates (Davies et al., 2016).

95 While there are currently no published occurrences of Kamchatkan tephra within Alaska, the large number of Kamchatkan-Kurile volcanoes active in the Holocene can also be considered as a potential source of distal cryptotephra, given prevailing wind directions and the large number of recorded major explosive eruptions (e.g. Braitseva et al., 1997; Kyle et al., 2011; Ponomareva et al., 2017). Transcontinental distribution of tephra from non-super  
100 eruptions has been established (e.g. Cook et al., 2018; Jensen et al., 2014), and Kamchatkan-sourced tephra have been traced to Greenland, Svalbard and the east coast of North America (van der Bilt et al., 2017; Cook et al., 2018; Mackay et al., 2016, Jensen et al., submitted).



Here, ages from Cascade Lake for three different chronostratigraphic techniques were visually compared and then modelled using Bayesian statistics to produce a composite age-depth model. Bayesian statistical techniques have been utilised in a wide range of fields to produce detailed age-depth models based on a relatively small number of dates (e.g. Christen et al., 1995; Litton and Buck, 1995) and, through their inclusion of additional (prior) information, they provide more precise interpolations than using raw dates alone (e.g. Blaauw and Christen, 2005; Bronk Ramsey, 2008).

## 2 Materials and Methods

Cascade Lake (68°22'48" N, 154°38'00" W; 990 m asl) lies on the north-central slope of the Brooks Range, the northernmost mountain range in Alaska (Fig. 1). Overall, the Brooks Range is located almost entirely above the Arctic Circle and represents a significant topographic barrier that divides the climatic influences of the Arctic and Pacific. The lake has an area of ~ 1 km<sup>2</sup> and a maximum depth of ~ 40 m in the main northwestern basin (Fig. 1b) with a total catchment size of ~10 km<sup>2</sup>. It presently has no significant inflow and one small outflow, west to Kurupa Lake (~ 920 m asl).

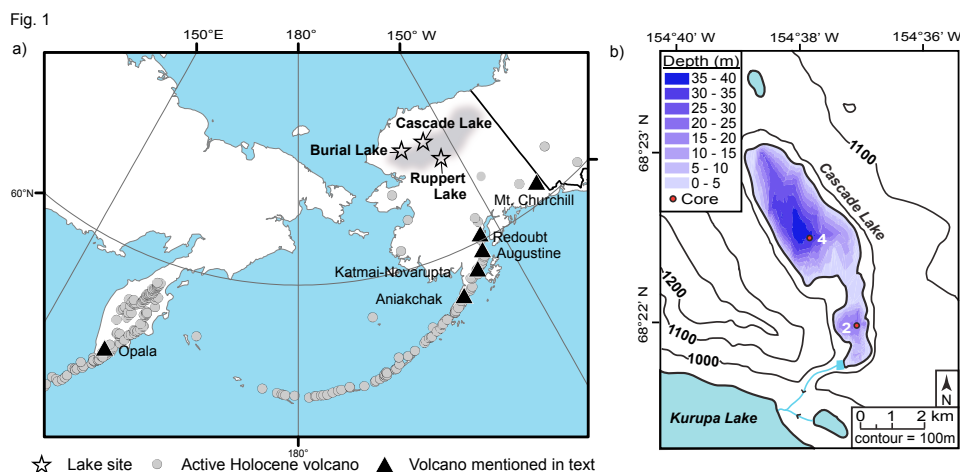


**Figure 1:** Location map showing Cascade Lake, coring sites, and other relevant locations and volcanoes mentioned in the text. Grey circles = active Holocene volcanoes (Global Volcanism Program, 2013); black triangles = volcanic sources mentioned in the text; grey shading = Brooks Range; star outlines = lakes mentioned in the text.

In 2013 sediment cores were collected from two sites at Cascade Lake using a percussion-piston coring system (long cores) and Aquatic Instruments universal corer (surface cores). Cores were split and described at the National Lacustrine Core Facility (LacCore) repository at the University of Minnesota, Twin Cities, and archive halves are



125 housed there. The 5.2-m-long composite sedimentary sequence, CASC-4A/2D, described by  
 Steen et al. (this volume) is the focus of the age-depth model reported here, which extends  
 down to the boundary with an underlying diamicton.

## 2.1 Previous geochronological data

### 2.1.1 Radiometric data

130 Radiometric data from Cascade Lake are detailed in full in Steen et al. (this volume)  
 and summarised here in Table 1. Eleven AMS  $^{14}\text{C}$  samples analysed at the University of  
 California-Irvine AMS Facility are reported. Samples consisted of terrestrial plant  
 macrofossils, insect parts, resting eggs, and aquatic vegetation as available. The oldest  
 sample analysed was from 350 cm composite depth, dating to  $\sim 15$  cal ka BP. Six  $^{210}\text{Pb}$   
 135 measurements were made from the uppermost sediment at Cascade Lake, but as equilibrium  
 ( $\sim 142$  yr BP) is reached within the top 4 cm of the cores these ages are not discussed in the  
 context of the Holocene age models.

140 **Table 1:** Radiometric ages from Cascade Lake (from Steen et al., this volume.). Ages are reported to the nearest whole year  
 ( $^{210}\text{Pb}$ ) or five years ( $^{14}\text{C}$ ) \* =  $^{14}\text{C}$  ages rejected as outliers; † = samples from surface core CASC-4B, all other samples are  
 from CASC-4A.

#### (a) $^{210}\text{Pb}$ CRS ages

Composite depth (cm)	Age (yr)	Error (yr)
0–0.5	23	1
0.5–1	48	1
1–1.5	67	2
1.5–2.25	83	2
2.25–3	112	4
3–3.5	143	7

#### (b) $^{14}\text{C}$ ages

Composite depth (cm)	Sample ID (UCIAMS #)	Age ( $^{14}\text{C}$ yr)	Error ( $^{14}\text{C}$ yr)	Material
2.6–4.6†	147384	170	30	Resting eggs, mixed aquatic fragments
5.5–7.5	134422*	1765	20	Insect remains, twigs, leaves, bryophyte, eggs
11–13†	147383	785	45	Leaf fragments, resting eggs, mixed aquatic fragments
30.5–32.5	131742	2825	25	Insect remains, moss fragments, resting eggs, fine unidentified pieces
85.75–87.75	128095	4160	120	Insect remains, twigs, leaves, bryophyte, resting eggs
138–140	131743	5085	20	Insect remains, moss fragments, resting eggs, fine unidentified pieces
197–199	131744	6485	25	Insect remains, moss fragments, resting eggs, fine unidentified pieces
233.5–235.5	134423	8270	35	Insect remains, twigs, leaves, resting eggs, fine unidentified pieces
245–248	128096*	13200	450	Insect remains, aquatic vegetation, twigs, resting eggs
303–304	131745	9875	35	Insect remains, moss fragments, resting eggs, fine unidentified pieces
348.5–351	137726	12690	150	Insect fragments, twig, leaf fragments



### 2.1.2 PSV ages

145 A composite inclination record and associated age model for Cascade Lake (Steen et  
 al., this volume) was produced using inclination age control points (tie-points) matched to  
 two geometric field models (CAL510k.1b, Korte et al., 2011; pfm9k.1b, Nilsson et al., 2014)  
 and a palaeomagnetic record from nearby Burial Lake (~ 200 km west along the Brooks  
 Range; Dorfman, 2013). PSV scenario 1 (PSV-1) was produced using 14 inclination tie-  
 150 points in total (Table 2) and successfully extends the age model for Cascade Lake back to  
 ~21 ka.

**Table 2:** The PSV-1 inclination age model data, with chronological tie-points calculated for Cascade Lake with Burial Lake, CAL510k1b and pfm9k1b. Reported ages are rounded to the nearest five years. See Steen et al. (this volume) for full details.

Tie Point	Composite depth (cm)	Burial Lake Age (cal yr BP)	Burial Lake Age 95% CI (cal yr BP)	CAL510k1b Age (yr BP)	+/-	pfm9k1b Age (yr BP)	+/-
I1	60	2270	1790-2765	2065	500	1955	500
I2	80	2755	2440-3045	2945	500	2635	500
I3	155	4810	4285-5345	4145	500	4195	500
I4	177	7275	7140-7415	5705	500	5435	500
I5	189	-	-	6165	500	6305	500
I6	203	-	-	6585	500	7145	500
I7	228	9880	9470-10280	7345	500	7655	500
I8	246	-	-	8185	500	8345	500
I9	284	11935	11440-12430	9425	500	-	-
I10	357	15455	14745-16155	-	-	-	-
I11	419	17055	16660-17430	-	-	-	-
I12	427	17415	16860-17960	-	-	-	-
I13	454	18130	17360-18930	-	-	-	-
I14	509	20520	19370-21630	-	-	-	-

155 The ages of tie-points from the geometric field models are based on a database of 75  
 selected sedimentary palaeomagnetic records from the SED12k data compilation (Donadini  
 et al., 2010; used by CAL510k.1b, Korte et al., 2011). The database was further parsed to  
 exclude bulk <sup>14</sup>C samples, archaeomagnetic data with large temporal uncertainties, and  
 palaeomagnetic behaviour incompatible with the majority of records during the Holocene  
 160 (pfm9k.1b, Nilsson et al., 2014). Both models have reported estimated temporal resolutions  
 of ± 500 a. Burial Lake tie-point ages and errors are derived from the <sup>14</sup>C age model of the  
 sediment cores (Dorfman, 2013), which is based on terrestrial macrofossils and shows  
 remarkably linear sediment accumulation over ~ 17 ka cal BP.

### 2.3 Cryptotephra analysis

165 Cryptotephra analyses are reported here from the past 4 ka, as a large number of the  
 most well-known, dated, and widely distributed tephra in Alaska were erupted during this  
 time period (Davies et al., 2016). This is also the interval when the <sup>14</sup>C ages in Cascade Lake



cores appear to be too old relative to the expected ages of the PSV features and therefore where tephra have significant potential to validate and improve a final age-depth model.

170 No visible tephra were located in cores from Cascade Lake (in fact, no visible beds are known north of the Brooks Range); targeted cryptotephra analyses were undertaken using contiguous 1-cm-thick subsamples from 1.42 m composite depth to the surface. Standard methods (e.g. Blockley et al., 2005) were used to produce glass shard concentration profiles throughout the two core sections and the heavy liquid, Lithium Heteropolytungstate (LST),  
175 was used for density separations. Glass shards for geochemical analysis were re-extracted from peaks in shard concentration using heavy liquid separation and samples were mounted in an epoxy puck and polished to expose glass surfaces before being carbon coated prior to electron probe microanalysis (EPMA). New data are reported here from glass shards analysed on a JEOL 8900 Superprobe at the University of Alberta by wavelength dispersive X-ray  
180 spectroscopy (WDS) following established protocols (e.g. Jensen et al., 2008, 2019).

A standard suite of ten elements (Si, Ti, Al, Fe, Mn, Mg, Ca, Na, K, Cl) was measured using a 5  $\mu\text{m}$  beam with 15 keV accelerating voltage and 6 nA beam current. This focussed beam (usually 10  $\mu\text{m}$  is utilised) can result in Na loss in more sensitive glasses (e.g. Jensen et al., 2019; Foo et al., 2020). However, where intensity data loss does occur, it has  
185 been shown that empirical corrections can be applied if the data demonstrate linear variance over time (Nielsen and Sigurdsson, 1981). Here Na, and if necessary, Si, were corrected for Time Dependent Intensity (TDI) loss (or gain) using a self-calibrated correction with Probe for EPMA software (Donovan et al., 2015).

Two secondary standards of known composition were run concurrently with all tephra  
190 samples: ID 3506, a Lipari rhyolite obsidian, and a reference sample of Old Crow tephra, a well-characterised, secondarily hydrated tephra bed (e.g. Kuehn et al., 2011). All results were normalised to 100% and are presented as weight percent (wt%) oxides. New major-element geochemical data and associated standard measurements, as well data points for relevant reference material (analysed concurrently, where possible), are reported in the Supplementary  
195 Information (Tables S1, S2).

#### 2.4 Bayesian age modelling

Three steps are detailed here for identifying and resolving problematic chronometer offsets using the data from Steen et al. (this volume) and new cryptotephra correlated ages. Firstly, ages that were obviously out of stratigraphic sequence were rejected previously by  
200 Steen et al. (this volume). Secondly, OxCal's Poisson process model (P\_Sequence, Bronk



Ramsey, 2008) was used to construct independent models for each chronometer. These were then visually compared to detect offsets between the dating methods. This is more effective than using statistical techniques as a first approach as they can be biased by datasets with high numbers of dates and tight distributions. Here, cryptotephra isochrons were used as independent checks for the other chronological methods, e.g. to identify  $^{14}\text{C}$  outliers.

Finally, the resulting chronological data were combined in one composite P\_Sequence model (OxCal v4.4; Bronk Ramsey, 2009). This set-up allows variable accumulation rates; here the k parameter (deposition events defined as increments per unit length, controlling model rigidity and resolution) was set as variable rather than fixed to increase model flexibility (Bronk Ramsey, 2013). General (Student's t) outlier analysis was used to identify any remaining anomalous ages in the parsed dataset. All ages were given the prior probability of 5% of ages being incorrect; if an age needs to be shifted substantially (by more than two standard deviations) to fit the resulting age-depth model it was identified as an outlier and downweighed in the process (Blockley et al., 2007).

### 215 3 Cryptotephra data

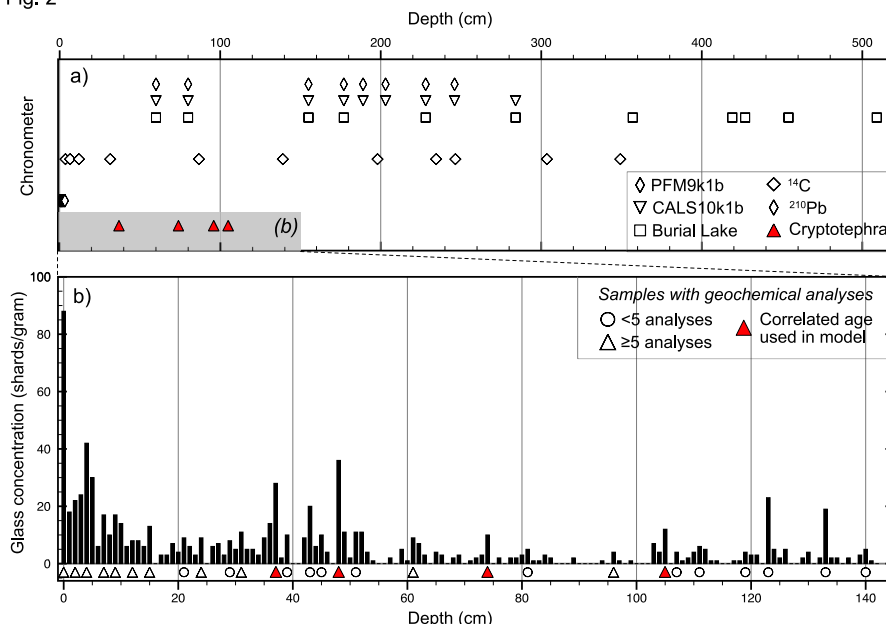
Glass shards were present in 75% of the samples analysed here. The composite shard concentration profile for the 1.42 m of counted samples is shown in Fig. 2. Twenty-eight peaks were chosen for geochemical analysis based on the relative abundances of shards counted at those depths. For each sample, geochemical analyses were performed on single grains, but 15 of the peaks chosen resulted in fewer than five shards exposed on the EPMA puck surface. This is likely due to the relatively low concentrations of glass present overall.

Of the remaining 13 samples, five have dominant unique geochemical populations (i.e. single eruptions are strongly represented), six have multiple identifiable trends/populations (representing an amalgamation of shards from multiple eruptions) and two have sparse shards with no discernible geochemical trends. Table 3 and Fig. 3 show the samples analysed, the average major element EPMA data for identified geochemical populations and any geochemical correlations to known eruptions with associated chronological data or similarities to known volcanic sources. Normalised single point major element EPMA datasets and associated standard analyses are provided in Tables S1 and S2.





Fig. 2



230

**Figure 2:** Cascade Lake core CASC-4A/2D multi-method chronological controls. (a) The composite depths of radiometric ages (<sup>14</sup>C and <sup>210</sup>Pb; Table 1), PSV-1 tie-points from three models (Table 2) and correlated cryptotephra ages (Table 4). The shaded grey area shows the depth interval of core sampled for cryptotephra analysis (expanded in panel b). (b) Glass shard concentration counts produced down to 145 cm, and the composite depths of analysed glass peaks. Circles = <5 points analysed; triangles = >5 points analysed; filled grey triangles have correlated ages that are used in the age-depth model.

235

### 3.1 Unique glass populations

Five samples contained glass shards that show dominant unimodal rhyolitic populations based on between 10 and 38 geochemical analyses. These are interpreted as primary tephra-fall events relating to contemporaneous eruptions (i.e. they show no evidence of secondary reworking). Four of these five samples can be used as isochrons as they correlate to reference material from known and dated eruptions (University of Alberta reference collection samples, Fig. 3; details provided in Tables 3 and S1). Key information regarding these eruptions and the tephra deposits are summarised in Table 4. Samples are discussed here individually from oldest to youngest and age estimates are given as two sigma calibrated age ranges unless otherwise stated.

245



**Table 3:** Average major element geochemical data for identifiable populations of analysed tephra samples and suggested correlations. (##) = standard deviation; FeOt = total iron oxide as FeO; H<sub>2</sub>O<sub>d</sub> = water by difference. (a) Samples used here as tie-points; (b) Reference material analysed at the University of Alberta, for full details regarding the original sample details please see listed references. (c) Samples with multiple populations or too few points to use as tie-points. Only groups of 3 or more analyses are shown here – for full details see Table S1.

**a) Samples used as tie-points**

Sample #	Popn	SiO <sub>2</sub>	TiO <sub>2</sub>	Al <sub>2</sub> O <sub>3</sub>	FeOt	MnO	MgO	CaO	Na <sub>2</sub> O	K <sub>2</sub> O	Cl	Total	H <sub>2</sub> O <sub>d</sub>	n	Correlation
CL-37	-	76.73 (0.26)	0.11 (0.03)	13.27 (0.12)	0.60 (0.09)	0.08 (0.03)	0.12 (0.02)	0.77 (0.04)	4.39 (0.23)	3.83 (0.22)	0.12 (0.02)	100.00 (0.00)	3.90 (1.31)	10	Opala (OP)
CL-48	a	74.52 (0.58)	0.22 (0.06)	14.12 (0.32)	1.49 (0.20)	0.06 (0.01)	0.34 (0.08)	1.57 (0.13)	4.07 (0.27)	3.35 (0.25)	0.34 (0.03)	100.00 (0.00)	2.23 (1.58)	10	Mt. Churchill – White River Ash (northern lobe, WRAn)
	b	77.76 (0.69)	0.16 (0.05)	12.43 (0.42)	1.06 (0.10)	0.04 (0.02)	0.15 (0.04)	0.91 (0.18)	3.65 (0.16)	3.61 (0.19)	0.30 (0.04)	100.00 (0.00)	2.25 (1.89)	12	
	all	76.29 (1.77)	0.19 (0.06)	13.20 (0.94)	1.26 (0.26)	0.05 (0.02)	0.24 (0.11)	1.21 (0.37)	3.84 (0.30)	3.49 (0.25)	0.31 (0.04)	100.00 (0.00)	2.24 (1.71)	22	
CL-74	-	74.16 (0.63)	0.30 (0.05)	13.91 (0.23)	1.96 (0.15)	0.11 (0.02)	0.46 (0.06)	2.18 (0.14)	4.81 (0.26)	1.91 (0.09)	0.25 (0.03)	100.00 (0.00)	0.48 (1.24)	36	Ruppert
CL-96	-	74.04 (0.95)	0.40 (0.03)	13.72 (0.46)	1.89 (0.15)	0.08 (0.02)	0.49 (0.09)	2.06 (0.18)	4.33 (0.23)	2.81 (0.08)	0.24 (0.02)	100.00 (0.00)	0.86 (1.18)	12	Unknown
CL-105	a	71.10 (0.29)	0.48 (0.03)	15.19 (0.15)	2.34 (0.07)	0.13 (0.02)	0.52 (0.03)	1.64 (0.04)	5.53 (0.23)	2.91 (0.12)	0.20 (0.02)	100.00 (0.00)	0.54 (0.93)	11	Aniakchak CFE II

**b) Reference material analyses from the University of Alberta**

Site	Sample ID	SiO <sub>2</sub>	TiO <sub>2</sub>	Al <sub>2</sub> O <sub>3</sub>	FeO <sub>t</sub>	MnO	MgO	CaO	Na <sub>2</sub> O	K <sub>2</sub> O	Cl	Total	H <sub>2</sub> O <sub>d</sub>	n	Correlation	Reference sample details
Duke River Fan, YT	UA 1044	74.32 (0.63)	0.21 (0.05)	14.18 (0.33)	1.54 (0.15)	0.06 (0.03)	0.32 (0.05)	1.67 (0.16)	4.11 (0.18)	3.26 (0.13)	0.33 (0.04)	100.00 (0.00)	2.40 (1.15)	55	White River Ash (northern lobe)	Jensen (2007)
Sixtymile River area, YT	UT 1480, Sample 16	73.95 (2.06)	0.21 (0.07)	14.38 (0.99)	1.50 (0.31)	0.06 (0.03)	0.35 (0.14)	1.77 (0.49)	4.29 (0.31)	3.23 (0.19)	0.34 (0.04)	100.00 (0.00)	2.82 (0.78)	31	White River Ash (northern lobe)	Preece <i>et al.</i> (2014), this paper
	UT 1482, Sample 17	73.65 (1.80)	0.23 (0.06)	14.50 (0.87)	1.59 (0.29)	0.06 (0.02)	0.38 (0.12)	1.83 (0.46)	4.26 (0.26)	3.25 (0.19)	0.34 (0.05)	100.00 (0.00)	3.06 (0.88)	34		
Zagoskin Lake, AK	UA 1602a	59.13 (0.97)	1.40 (0.07)	16.45 (0.16)	7.50 (0.64)	0.22 (0.03)	2.97 (0.22)	6.06 (0.40)	4.61 (0.26)	1.57 (0.11)	0.13 (0.02)	100.00 (0.00)	2.30 (1.07)	17	Aniakchak CFE II (andesite, rhyodacite)	Ager (2003); Davies <i>et al.</i> (2016)
	UA 1602b	71.07 (0.52)	0.50 (0.05)	15.19 (0.28)	2.55 (0.03)	0.14 (0.03)	0.51 (0.08)	1.78 (0.19)	5.07 (0.29)	3.05 (0.13)	0.19 (0.02)	100.00 (0.00)	2.48 (1.56)	32		
Ruppert Lake, AK	UA 2557	74.08 (0.39)	0.30 (0.05)	13.96 (0.16)	2.00 (0.12)	0.10 (0.03)	0.46 (0.04)	2.18 (0.10)	4.80 (0.14)	1.93 (0.10)	0.22 (0.02)	100.00 (0.00)	0.53 (0.90)	17	Ruppert	Monteath <i>et al.</i> (2017)
Southern Kamchatka	UA 3286	76.65 (0.20)	0.12 (0.04)	13.31 (0.12)	0.69 (0.03)	0.11 (0.03)	0.12 (0.02)	0.77 (0.03)	4.24 (0.11)	3.91 (0.09)	0.11 (0.02)	100.00 (0.00)	2.65 (0.71)	30	Opala (Phase III)	Andrews <i>et al.</i> (2018)



Table 3: *cont.*  
 c) Other samples analysed

Sample	Popn	SiO <sub>2</sub>	TiO <sub>2</sub>	Al <sub>2</sub> O <sub>3</sub>	FeOt	MnO	MgO	CaO	Na <sub>2</sub> O	K <sub>2</sub> O	Cl	Total	H <sub>2</sub> O <sub>d</sub>	n
CL-0	a	71.02 (0.29)	0.48 (0.03)	14.90 (0.15)	2.36 (0.08)	0.16 (0.03)	0.50 (0.02)	1.67 (0.05)	5.64 (0.26)	3.09 (0.08)	0.23 (0.03)	100.00 (0.00)	1.46 (1.26)	7
	b	74.42 (1.46)	0.16 (0.04)	13.99 (0.76)	1.28 (0.28)	0.05 (0.02)	0.32 (0.12)	1.57 (0.29)	4.63 (0.13)	3.33 (0.12)	0.33 (0.01)	100.00 (0.00)	3.12 (1.59)	3
	c	74.68 (0.84)	0.32 (0.04)	13.68 (0.67)	2.02 (0.16)	0.09 (0.02)	0.46 (0.04)	2.22 (0.19)	4.43 (0.34)	1.94 (0.05)	0.21 (0.06)	100.00 (0.00)	1.78 (0.62)	6
CL-1	d	75.63 (1.35)	0.26 (0.10)	13.51 (0.44)	1.22 (0.41)	0.05 (0.01)	0.31 (0.10)	1.30 (0.38)	4.54 (0.45)	3.05 (0.19)	0.15 (0.07)	100.00 (0.00)	2.32 (1.05)	6
	e	76.91 (0.45)	0.33 (0.04)	12.27 (0.09)	1.57 (0.11)	0.03 (0.01)	0.26 (0.02)	1.16 (0.02)	4.33 (0.33)	2.97 (0.01)	0.21 (0.01)	100.00 (0.00)	1.61 (0.48)	3
	a	71.00 (0.59)	0.49 (0.10)	15.00 (0.23)	2.48 (0.34)	0.14 (0.03)	0.52 (0.10)	1.68 (0.20)	5.42 (0.16)	3.11 (0.14)	0.22 (0.03)	100.00 (0.00)	1.35 (0.78)	14
CL-2	b	73.73 (0.35)	0.21 (0.02)	14.46 (0.23)	1.51 (0.05)	0.04 (0.03)	0.37 (0.03)	1.77 (0.10)	4.52 (0.12)	3.13 (0.08)	0.33 (0.02)	100.00 (0.00)	2.81 (1.14)	5
	c	74.17 (0.45)	0.32 (0.03)	13.75 (0.16)	1.94 (0.08)	0.12 (0.02)	0.45 (0.01)	2.20 (0.18)	4.82 (0.23)	2.03 (0.04)	0.26 (0.01)	100.00 (0.00)	1.14 (0.74)	4
	d	75.86 (0.27)	0.25 (0.04)	13.18 (0.14)	1.56 (0.05)	0.07 (0.03)	0.31 (0.04)	1.66 (0.11)	4.96 (0.14)	2.01 (0.03)	0.17 (0.02)	100.00 (0.00)	2.04 (0.28)	4
CL-4	e	76.90 (1.24)	0.26 (0.16)	12.63 (0.35)	1.19 (0.52)	0.07 (0.02)	0.22 (0.12)	1.05 (0.38)	4.20 (0.23)	3.35 (0.34)	0.18 (0.11)	100.00 (0.00)	3.07 (0.93)	5
	a	66.61 (1.64)	0.77 (0.26)	15.68 (0.22)	4.45 (1.07)	0.13 (0.05)	1.19 (0.14)	3.50 (0.44)	4.88 (0.3)	2.63 (0.12)	0.20 (0.11)	100.00 (0.00)	1.79 (0.79)	4
	b	70.86 (0.86)	0.49 (0.04)	15.00 (0.17)	2.47 (0.35)	0.14 (0.03)	0.51 (0.08)	1.69 (0.18)	5.50 (0.36)	3.17 (0.3)	0.22 (0.02)	100.00 (0.00)	1.09 (0.91)	15
CL-7	c	76.71 (0.16)	0.12 (0.04)	13.26 (0.02)	0.61 (0.17)	0.12 (0.03)	0.09 (0.06)	0.72 (0.03)	4.25 (0.18)	4.07 (0.36)	0.10 (0.04)	100.00 (0.00)	2.78 (0.86)	3
	a	70.93 (0.19)	0.48 (0.02)	15.03 (0.12)	2.36 (0.09)	0.13 (0.04)	0.59 (0.13)	1.88 (0.38)	5.40 (0.45)	3.03 (0.20)	0.20 (0.03)	100.00 (0.00)	1.04 (0.15)	5
	b	75.83 (0.61)	0.23 (0.05)	13.31 (0.39)	1.55 (0.04)	0.07 (0.03)	0.33 (0.08)	1.67 (0.24)	4.82 (0.23)	2.06 (0.1)	0.16 (0.04)	100.00 (0.00)	1.63 (0.62)	6
CL-31		77.92 (0.7)	0.13 (0.02)	12.22 (0.55)	1.06 (0.1)	0.06 (0.03)	0.15 (0.04)	0.85 (0.23)	3.84 (0.34)	3.53 (0.26)	0.31 (0.01)	100.00 (0.00)	1.97 (1.16)	6
	a	71.23 (0.80)	0.43 (0.04)	15.05 (0.28)	2.39 (0.07)	0.15 (0.02)	0.44 (0.05)	1.57 (0.13)	5.50 (0.56)	3.09 (0.19)	0.20 (0.02)	100.00 (0.00)	-0.28 (0.28)	3
	b	77.70 (0.33)	0.21 (0.02)	12.72 (0.20)	1.23 (0.07)	0.05 (0.03)	0.34 (0.01)	2.05 (0.05)	4.01 (0.16)	1.62 (0.09)	0.10 (0.02)	100.00 (0.00)	0.44 (1.40)	4
CL-105	b	71.81 (0.55)	0.51 (0.09)	14.75 (0.03)	2.32 (0.22)	0.10 (0.02)	0.41 (0.05)	1.43 (0.13)	4.85 (0.22)	3.69 (0.04)	0.17 (0.01)	100.00 (0.00)	0.37 (0.14)	4



255 **Table 4:** Cascade Lake cryptotephra and their suggested correlative eruptions. Age estimates for the core depth of the cryptotephra from Steen et al. (this issue) are compared with published ages for the listed eruptions. Bayesian modelled ages for both Aniakchak CFE II and Opala are updated here using OxCal and IntCal20.

Sample (Lab #)	Suggested correlation		Cascade Lake age estimates (95% range)		Age estimate for correlated eruption			
	Tephra	Source volcano	<sup>14</sup> C (cal yr BP)	PSV-1 (yr BP)	95% range (cal yr BP)	Method	Deposit type	Age estimate reference(s)
CL-37 (UA3721)	OP	Opala, Kamchatka	3180-2300	1720-990	1395-1305	Calibrated <sup>14</sup> C (IntCal20)	Visible tephra (Kamchatka)	Braitseva et al. (1995); updated here using IntCal20
CL-48 (UA3730)	WRAn	Mt. Churchill, Alaska	3895-2935	2110-1360	1689-1540	Calibrated <sup>14</sup> C (IntCal20)	Visible tephra (Alaska, Yukon)	Reuther et al. (2020)
CL-74 (UA3733)	Ruppert	Unknown (likely Alaska)	4920-4145	2795-2280	2800-2130	Calibrated <sup>14</sup> C (IntCal20)	Distal cryptotephra (four bogs - Newfoundland, Canada; Maine, Michigan, New York, USA)	Jensen et al. (submitted)
CL-96 (UA3735)	-	Unknown	5345-4840	3355-2600	-	-	-	-
CL-105a (UA3736)	CFE II	Aniakchak, Alaska	5460-5030	3525-2675	3590-3545	Calibrated <sup>14</sup> C (IntCal20) & ice core	Visible tephra (Alaska) and cryptotephra (Alaska, USA; Newfoundland, Canada)	Davies et al. (2016); updated here using IntCal20
					3572 ± 8 (-20 ± 5)	GICC05 (with correction)	Distal cryptotephra (NGRIP, Greenland)	Vinther et al. (2006); Adolphi & Muscheler (2016); Pearce et al. (2017)



Fig. 3

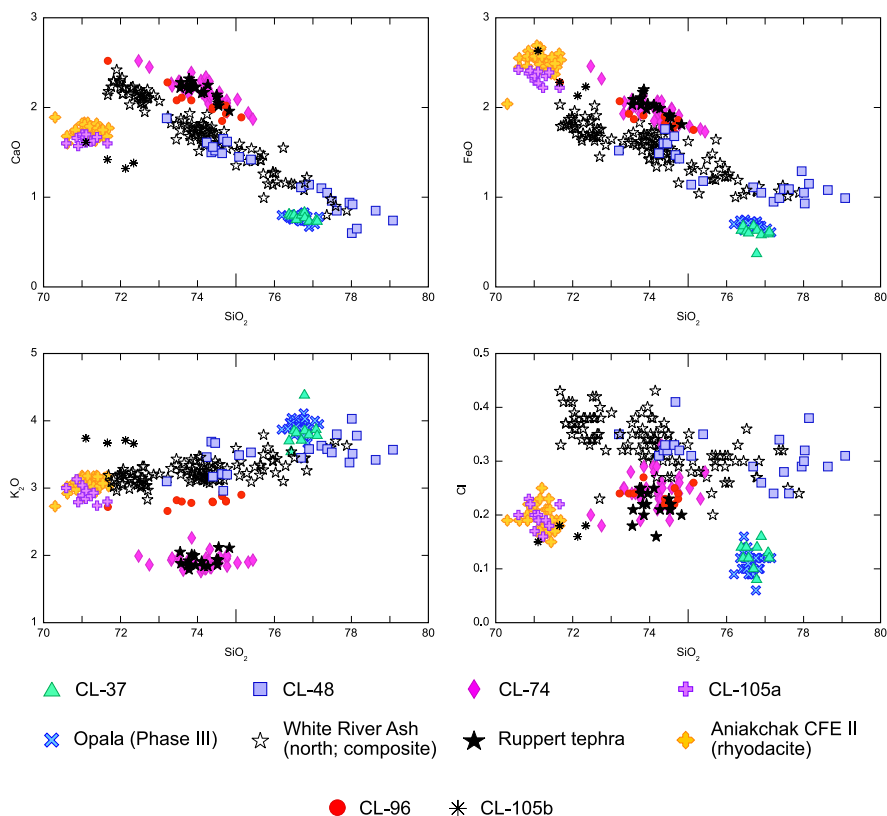


**Figure 3:** Geochemical biplots showing major element data for the five unique populations of cryptotephra glass identified from Cascade Lake sediment, and data for reference material where relevant. Points for CL-105b are also plotted, for reference. See Table 3 for sample details and Table S1 for point data.

### 260 3.1.1 CL-105 (Aniakchak Caldera Forming Eruption II)

CL-105, a peak concentration of 12 shards/gram, is a geochemical match for the rhyodacite population of the widespread Late Holocene caldera forming eruption of Aniakchak (CFE II) (Fig. 3; Bacon et al., 2014; Neal et al., 2001; Riehle et al., 1987). Tephra from this eruption have been found visibly across southern and western Alaska, and as  
 265 cryptotephra in the Bering Sea, Yukon, Newfoundland and Greenland (Davies, 2018; Denton and Pearce, 2008; Pearce et al., 2017, 2004; Ponomareva et al., 2018; Pyne-O'Donnell et al., 2012). A second population of four points was also identified in this sample (CL-105b, Table 3c), however it is unclear if these represent a separate event or alkali loss from the main population.



270 Chronologically, Aniakchak CFE II has been dated with radiocarbon from sequences  
with visible tephra and distal lakes and peat bogs with correlated cryptotephra, as well as  
with a precise ice-core model age estimate from distal cryptotephra identified in Greenland  
ice cores. The latter is supported using geochemically correlated glass shards as well as  
sulphate peaks and tree ring perturbations recorded in this interval (Coulter et al., 2012;  
275 McAneney and Baillie, 2019; Pearce et al., 2004). Glass shards correlated to the eruption in  
two NGRIP intervals have overlapping associated ice-core modelled ages of 3594-3589 yr  
BP (1641-1639 BCE – QUB-1198, 1644-1643 BCE – QUB 1201; Coulter et al., 2012;  
Vinther et al., 2006). When a correction factor of  $-19 \pm 3$  a (Adolphi and Muscheler, 2016) is  
applied to the GICC05 chronology, the resulting NGRIP modelled age for the eruption is  
280  $3572 \pm 4$  cal yr BP (Pearce et al., 2017).

Here we report updated modelled eruption ages produced using the Tau\_Boundary  
function in OxCal v.4.4 with IntCal20 (following Davies et al., 2016; Fig. S1, see Table S4  
for details). The ice-core chronology age discussed above is only compatible with published  
 $^{14}\text{C}$  ages if two of the three  $^{14}\text{C}$  ages that underlie the tephra in an exposed peat section in  
285 northwest Alaska (Blackford et al., 2014) are removed as outliers. This is unexpected because  
the peat section is one of the most precisely dated terrestrial sequences for Aniakchak CFE II,  
with six samples analysed at 0.5 cm increments over 3 cm immediately surrounding the  
tephra. While there are no obvious reasons for disregarding these two ages, beyond the  
disagreement with the ages from the ice cores, in this instance it seems pertinent to do so.  
290 Modelled Tau\_Boundary estimates for the eruption age are: a) 3545-3425 cal yr BP when all  
 $^{14}\text{C}$  dates are included, b) 3610-3450 cal yr BP with two  $^{14}\text{C}$  dates removed, and c) 3590-  
3545 cal yr BP including all but two  $^{14}\text{C}$  dates and the NGRIP ice core chronology age (Fig.  
S1). At Cascade Lake, using either the ice core chronology age estimate of  $3572 \pm 4$  cal yr  
BP (Adolphi and Muscheler, 2016; Pearce et al., 2017) or the Tau\_Boundary model age (c,  
295 above) for Aniakchak CFE II shows that while neither estimated age for this depth from  
Steen et al. (this volume) overlaps here, the PSV-1 age model is substantially closer than the  
 $^{14}\text{C}$  age model (Table 4).



### 3.1.2 CL-96 (unknown)

CL-96 represents a small peak of only four shards/gram but yielded 10 analytical  
300 points that have relatively high values for wt% TiO<sub>2</sub>, FeO and CaO (Table 3a). These  
analyses are similar to CL-74 for many major elements, but have substantially higher wt.%  
K<sub>2</sub>O (2.81 wt.% average vs. 1.91 wt.%, respectively). The shards are likely from a source in  
Alaska and the Aleutian Arc and are similar to published average analyses for glass from the  
Katmai volcanic cluster (Fierstein, 2007) but cannot be directly correlated here to a particular  
305 vent or eruption. Therefore, there are no associated age estimates that can be used here to  
compare with other Cascade Lake chronometers.

### 3.1.3 CL-74 (Ruppert tephra)

CL-74 has a shard concentration peak of 10 shards/gram but a disproportionately high  
number of analyses (38) when compared to other samples. This rhyolitic population of platy  
310 and cusped shards has distinctly low wt.% K<sub>2</sub>O values (~2.0%) compared to other tephra  
from Alaska and is a geochemical match for the Ruppert tephra. This tephra was first  
identified in Newfoundland (NDN-230; Pyne-O'Donnell et al., 2012) and tentatively  
correlated to Augustine G, although this is now known to be incorrect (Blockley et al., 2015;  
Monteath et al., 2017). While it is geochemically similar to glass from Mt. Augustine, no  
315 proximal relative is currently known. The tephra was later found in, and subsequently  
named after, Ruppert Lake, directly south of Cascade Lake on the southern slope of the  
Brooks Range (Monteath et al., 2017) and has also been identified in peatlands in the Yukon  
(Davies, 2018) and eastern USA (Jensen et al., submitted).

Chronologically, Ruppert Lake's <sup>14</sup>C age model shows evidence of old carbon  
320 contamination (Monteath et al., 2017) but Jensen et al. (submitted) produced a modelled two-  
sigma age of 2800-2130 cal yr BP using <sup>14</sup>C ages from four distal peat bogs (located in  
Newfoundland, Canada; Maine, Michigan and New York, USA). This agrees well with Steen  
et al.'s (this volume) PSV-1 age estimate for this depth (Table 4).

### 3.1.4 CL-48 (White River Ash, northern lobe)

325 CL-48 is the largest glass concentration peak of the pre-19<sup>th</sup> century sequence, with  
36 shards/gram. These pumaceous rhyolitic shards are geochemically similar to the White



River Ash, which comprises two Late Holocene eruptions from Mt. Churchill (Lerbekmo, 2008; Preece et al., 2014). Major element glass geochemical data for these eruptions are very similar (with substantial overlap) but given the broad range of wt.% SiO<sub>2</sub> values and bimodal  
330 geochemistry of CL-48 shards, it likely correlates with the older northern-focused eruption (WRAn). The tephra from this eruption is more geochemically diverse than that of the younger eastern lobe (Davies et al., 2019) and is preserved as a visible bed in sediment deposits north of the vent in Alaska and the Yukon. Reference geochemical data from three  
335 WRAn samples in the Yukon (Jensen, 2007; Preece et al., 2014) are plotted in Fig. 3 to demonstrate the observed variability; distal correlatives trend towards higher wt.% SiO<sub>2</sub> values compared to proximal samples (Davies et al., 2019).

WRAn has a recently updated modelled two-sigma <sup>14</sup>C age of 1689-1560 cal yr BP (Reuther et al., 2020). This is slightly younger than previous published estimates (e.g. 1805-1605 cal yr BP, Davies et al., 2016) as the new ages and modelling methods reported by  
340 Reuther et al. (2020) better constrain the eruption, which occurred at a time when there is a fluctuation in the <sup>14</sup>C calibration curve. This age is in good agreement with Steen et al.'s (this volume) PSV-1 age estimate for this depth (Table 4).

### 3.1.5 CL-37 (OP tephra)

CL-37 is the second largest pre-19<sup>th</sup> century peak, with 28 shards/gram. This rhyolite  
345 is distinctive from published analyses of glass from Alaska, with notably low wt.% FeO<sub>t</sub> (average 0.60%) and CaO (average 0.77%). This characteristic geochemical signature has been observed in some volcanic glasses from Kamchatka (e.g. Portnyagin et al., 2020). CL-37 is shown here to correlate with the Late Holocene caldera forming eruption of Opala (OP), Kamchatka (e.g., Andrews et al., 2018; Braitseva et al., 1995, 1997; Kyle et al., 2011;  
350 Melekestsev et al., 1992; Plunkett et al., 2015). CL-37 is the first ultra-distal correlation of glass from this eruption outside of Kamchatka.

Here we report an updated modelled eruption age for OP of 1395-1305 cal yr BP (Fig. S2). This was produced using the Tau\_Boundary function in OxCal v4.4 with IntCal20 following the methodology of Davies et al. (2016) with <sup>14</sup>C ages reported in (Braitseva et al.,  
355 1995) (Table S4). This is in good agreement with previous published ages for the eruption and with Steen et al.'s (this volume) PSV-1 age estimate for this depth (Table 4).





### 3.2 Multimodal/mixed glass populations

Glass shards from six of the remaining analysed shard-frequency peaks have mixed or multimodal geochemical data and two have scattered results with no discernible trend. Higher levels of background shards are present from 35 cm to the surface, and the geochemical ‘noise’ is also particularly evident in the youngest samples, with all peaks analysed in the past millennium showing either multimodal or scattered data. Geochemical biplots for samples with multiple populations of only a few shards (CL-0, -2, -31, -61) are shown in full in Fig. S3.

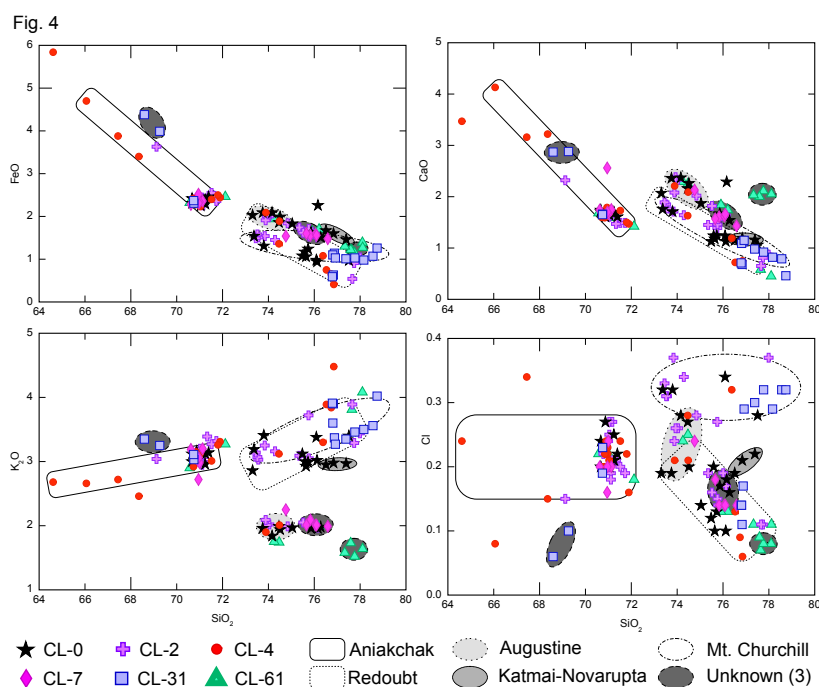
CL-61 is the only analysed mixed sample that pre-dates the past millennium, located between the Ruppert (CL-74, 2800-2130 cal yr BP) and WRAn (CL-48, 1689-1560 cal yr BP) tephtras. It contains a few shards that are similar to the rhyodacite from Aniakchak volcano and also Augustine tephra (Fortin et al., 2019; Waitt and Begét, 2009), but while these volcanoes have known activity at this time (e.g. Bacon et al., 2014; Waitt and Begét, 2009) there are not enough analyses available for a definite correlation.

Of the six mixed samples, only two – CL-4 and CL-7 – have populations that can be identified as dominant from the analyses presented here. Rhyodacitic and dacitic glass shards from these samples overlap geochemically with reference data for Aniakchak (Davies et al., 2016) and are interpreted as strong evidence of eruptive activity at Aniakchak, given both the number of shards and the proportion of analyses that they represent. CL-7 also has six points that are geochemically similar to an Early Holocene eruption, KO (~8410-8455 cal yr BP; Braitseva et al., 1997) from Kamchatka, but this does not correlate to any known eruptions from Kamchatka in the timeframe of this deposit. While these are the three most coherent geochemical populations observed in these mixed samples, they are not deemed useful here for chronostratigraphic applications (discussed further in Sect. 5.1.1).

An alternative approach for considering these mixed data is to parse by geochemical trend rather than by individual sample. Given the high levels of background shards it is possible that the chosen shard concentration peaks do not relate directly to primary tephra-fall. This is particularly likely where multiple eruptive events are closely spaced and overlap. As each sample might contain shards from multiple eruptions these data can be seen as recording eruptive activity in a broader period, instead of discrete eruptions or accurately dated events.



Using this source-based classification, it is possible to identify eight geochemical groups, illustrated in Fig. 4, for the six mixed samples from the past ~1000 years. Five of these eight geochemical groups correlate with reference glass data for volcanic sources in Alaska (Aniakchak, Mt. Churchill, Redoubt, Augustine, Novarupta-Katmai). These volcanoes all have known eruptions or suspected eruptive activity over this time period (Alaska Volcano Observatory, 2016).



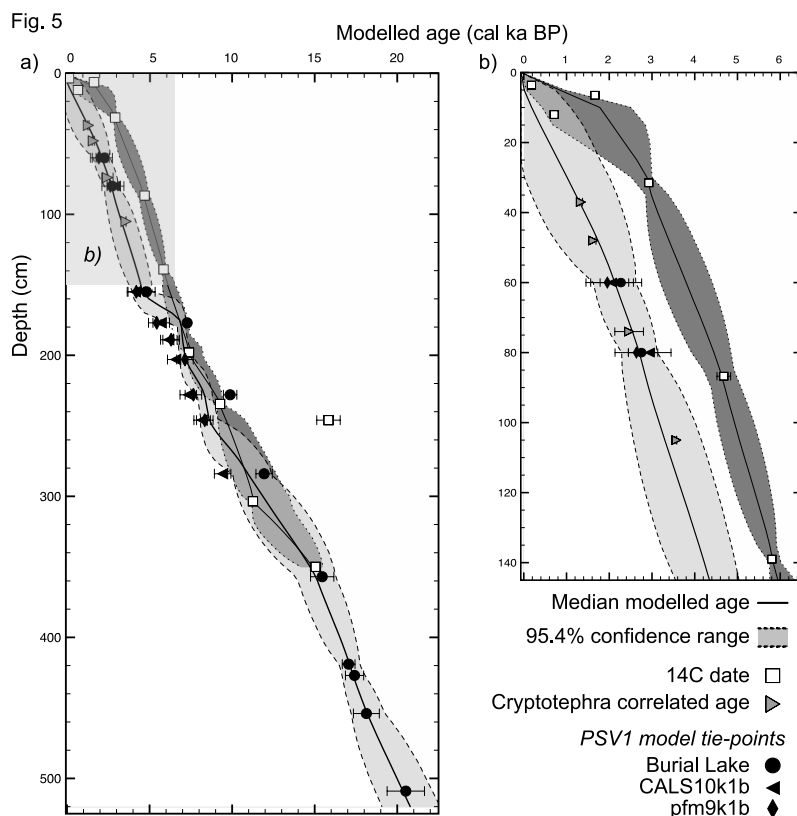
395 **Figure 4:** Geochemical biplots showing mixed-glass samples from Cascade Lake. Bounding shapes represent simplified geochemical fields for potential source volcanoes (to aid visualisation). For the full glass geochemical-data ranges associated with these volcanic sources see, e.g., Bolton et al. (2020), Davies et al. (2016), Fortin et al. (2019), Zander et al. (2018). Three populations with unknown sources are also shown using the same bounding line and fill. All single point analysis data are listed in Table S1.

#### 400 4 Bayesian age modelling

Step one of our chronometer comparison (see Sect. 2.4) considered if the individual ages fit their expected stratigraphic order. Steen et al. (this volume) noted that two  $^{14}\text{C}$  ages (5.5-7.5 cm and 245-248 cm) were out of sequence as they are anomalously old compared to their surrounding ages. They were therefore excluded from further consideration.



405 For step two of our comparison, an initial overlay of the individually modelled  
 chronometers (Fig. 5) showed that there are substantial offsets between  $^{14}\text{C}$  and PSV-1  
 models above 175 cm, as noted by Steen et al. (this volume). As outlined in Sect. 3.1 and  
 Table 4, the four available cryptotephra correlated ages agree well with PSV-1 tie-points  
 (Fig. 5b) and three further  $^{14}\text{C}$  ages (32.5-30.5 cm, 87.75-85.75 cm and 140-138 cm) are  
 410 therefore also removed as outliers. From 180-290 cm there is also a noticeable divergence  
 between the PSV data model tie-points used from geomagnetic field models and the Burial  
 Lake record (Fig. 5a).



415 **Figure 5:** Cascade Lake core CASC-4A/2D multi-method chronometer comparison of downcore age models based on PSV-1 tie-points (light grey shading) and radiocarbon ages (dark grey shading). 2 sigma uncertainties are plotted for all samples; where bars are not visible the uncertainty is smaller than the symbol (values in Table S3). Correlated tephra ages are overlain at their identified depths and show good agreement with the PSV-1 model. (a) Whole model down to 520 cm. Note disagreement between the geomagnetic field model and Burial Lake tie-points from 284-177 cm. PSV-1 model is extrapolated from 520-509 cm (from the base of the unit to the lowest dated sample); (b) enlarged 145 cm section, highlighted with the grey shaded box in panel a, showing cryptotephra correlated ages and the substantial offsets between  $^{14}\text{C}$  and PSV-1 age models.

420



For step three, a composite P\_Sequence model was produced using the PSV-1 tie-point ages, the four cryptotephra correlated ages and the six remaining  $^{14}\text{C}$  ages (details for OxCal input are given in File S1). This age-depth model was run with a Student's t-test outlier model, which identified four ages with strong likelihoods of being outliers (posterior values of 68-100; Fig. S4). These include two further  $^{14}\text{C}$  ages (199-197 cm and 235.5-233.5 cm) and two PSV tie-points from Burial Lake (177 cm and 228 cm). The 284 cm composite depth tie-point from Burial Lake was also removed as it failed the chi-squared test when combined with the tie-point from the pfm9k1b field model and was significantly older than the model results for that depth. These five ages are not included in the final version of the age-depth model presented here, as their removal improved the model agreement and reduced the associated uncertainties (Fig. S5).

Figure 6 shows the final age model, which uses 14 PSV-1 tie points, four cryptotephra correlated ages and four  $^{14}\text{C}$  ages to cover 509 cm of core. Ages are extrapolated from 509 cm, the composite depth of the lowest PSV-1 tie-point, to 520 cm, a unit boundary with underlying diamicton. Hence, a well-resolved age model was produced using a combination of ages from three independent chronometers and Bayesian statistical techniques.

## 5 Discussion

The data reported here have implications for cryptotephra records in northwestern North America and for Arctic sedimentary sequences and age models through the successful application of PSV dating over the last ~ 21 ka.

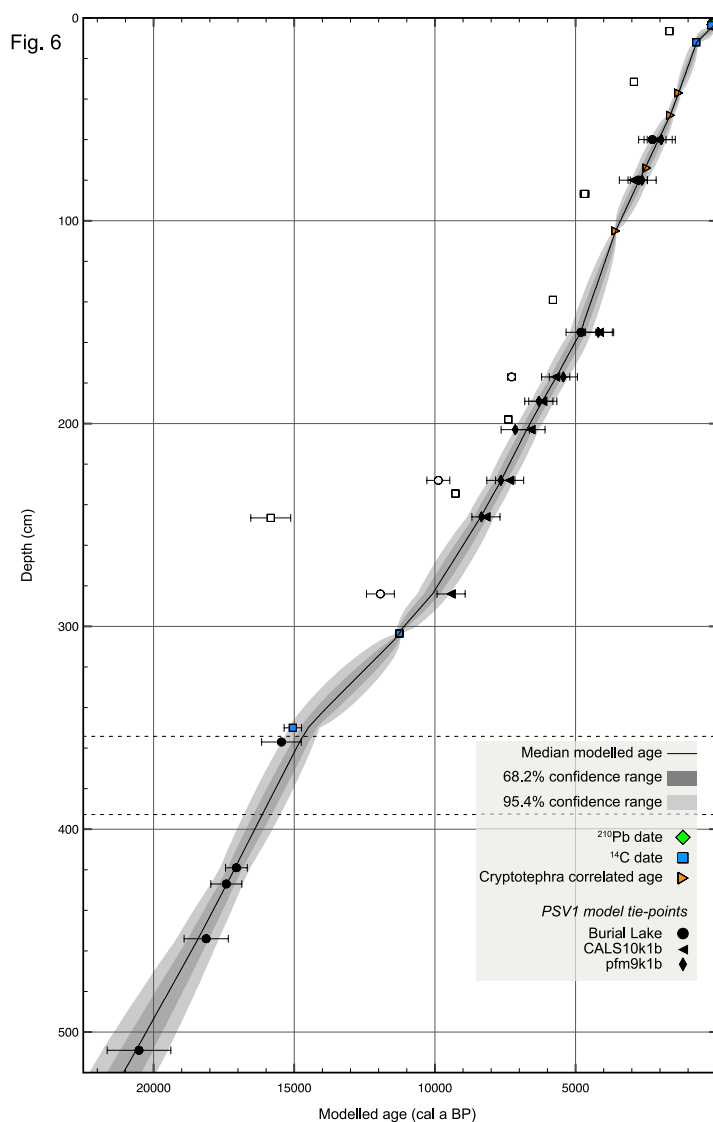


**Figure 6:** Age-depth plot showing the final Bayesian age model for Cascade Lake composite core CASC-4A/2D. Shaded areas show the 1 sigma (68.2%) and 2 sigma (95.4%) confidence ranges. Filled symbols are included in the model and white symbols are identified as outliers. 2 sigma errors are included for all ages; where they are not visible the error is smaller than the symbol used. Full details and values can be found in Table S3.

445

### 5.1 Cryptotephra in Arctic Alaska

This study demonstrates that identifiable concentrations of volcanic glass reach the north flank of the Brooks Range and can be used as chronostratigraphic tools where clear evidence of primary tephra-fall is preserved. In particular, this is the first report of ultra-distal



450 glass from the Late Holocene eruption of Opala, Kamchatka, as well as an unknown tephra,  
CL-96, likely from a source in the Alaska Peninsula or Aleutian Arc. Ruppert tephra and  
Aniakchak CFE II are both documented on the southern slope of the Brooks Range  
(Monteath et al., 2017), and their distributions are expanded here across this large  
topographic barrier. This is also the first distal identification of WRAn this far to the  
455 northwest of Mt. Churchill.

While the cryptotephra profile here only covers the Late Holocene, it highlights  
eruptive events that are both locally important and widespread and provides possibilities for  
correlating proxy data within North America and across the Pacific in Kamchatka. Our focus  
was specifically on the past ~4 ka as there are several widespread, well-dated and  
460 geochemically characterised tephra within Alaska during this time period. From 12-4 ka,  
there is a paucity of well-dated regional tephra that are documented and fully characterised,  
but it is possible that new tephra from other regions may be identified, as here with OP.

Compared to the cryptotephra stratigraphies published in Monteath et al. (2017) from  
Ruppert Lake and Woody Bog Pond, located ~150 km south of Cascade Lake on the southern  
465 slope of the Brooks Range, large differences can be seen in both the number of primary  
tephra preserved and the overall shard presence and concentrations. Reported glass  
abundances at the southern sites are at least an order of magnitude higher than those from  
Cascade Lake (100s – 1000s vs 10s shards/gram or less). This likely relates in part to the  
topographic barrier presented by the Brooks Range, causing increased rain-out of shards  
470 being transported from the south (e.g. in north trending plumes from Aniakchak CFE II) and  
deposition of shards before they reach the northern slope. Other factors may include lake size  
and bathymetry, catchment size, local topography and hydrology. Cascade Lake is an order  
of magnitude larger and deeper than the southern sites and hence has a larger surface area (~1  
km<sup>2</sup> vs 0.04 and 0.01 km<sup>2</sup>) but its catchment area is not proportionally larger (~10 km<sup>2</sup> vs <4  
475 km<sup>2</sup>) and it has no current inflow.

There are common issues affecting cryptotephra research in Alaska that still apply at  
this distal, Arctic site. The shard concentration profile reported for Cascade Lake is affected  
by closely spaced eruptions from multiple sources combined with relatively low sediment  
accumulation rates, causing geochemically variability within individual samples. The  
480 presence of glass in the majority of samples analysed shows a level of background deposition



that must be considered when interpreting data from identified shard concentration peaks. This is particularly important here as the signal:noise ratio between the peaks that have been correlated with known eruptions and the (fairly consistent) background shard concentration is relatively high. This is mostly due to the low concentrations of shards in the identified peaks,  
485 compared to other cryptotephra records in the area.

### 5.1.1 Multi-modal samples and historical activity

The issue of ‘clear evidence of primary tephra-fall’ being preserved is one that affects all cryptotephra records. Low numbers of shard analyses cannot be interpreted as conclusive evidence of an eruption, especially if multiple geochemical populations or trends are  
490 observed. This appears to only be a problem for certain parts of the Cascade Lake tephrostratigraphic record; there are discernible changes in shard concentrations and samples from the younger portion of the core contains multiple geochemical populations/trends. For example, samples analysed from 30-0 cm have multiple geochemical populations, which are not frequently seen below this. However, this view may be biased by the relatively higher  
495 number of samples with more than five analyses in this period. Also, the overall shard-concentration profile over the top 15 cm of the core has higher average and peak shard concentration values than the rest of the analysed sediment. These differences could be the result of a myriad of regional (e.g. eruption style, plume altitude, wind direction and strength, shard characteristics) and local (e.g. fallout on snow, sediment accumulation, hydrology,  
500 bioturbation) factors that affect the distribution, deposition, reworking, and ultimately preservation of shards. A succinct summary for these factors relating to cryptotephra in peatlands is given in Watson et al., (2015), and is largely applicable for lake sediments.

Beyond the five clearly defined cryptotephra samples, we present evidence here of volcanic activity using glass that is geochemically similar to reference data for Mt.  
505 Augustine, Redoubt, Aniakchak, Mt. Churchill, Novarupta-Katmai (e.g. Bolton et al., 2020) and further possible sources in Kamchatka and Alaska. Focusing on the modern period, this is interpreted as evidence for trace amounts of glass reaching the north flank of the Brooks Range from known eruptions, but without the resolution to interpret individual eruptive events. These shards are unlikely to represent significant reworking from the surrounding  
510 landscape, or within the lake sediment itself, as there is little ash in the area. This supposition



is supported by the record of known eruptions in the past millennium, including Novarupta-Katmai 1912, six eruptions from Redoubt and 13 from Augustine (Alaska Volcano Observatory, 2016).

Furthermore, sedimentation rates calculated from the age-model data using OxCal  
515 v4.4 (Table S3) show that there is a significant decrease, by ~50%, for the depth interval of  
12-4 cm (~1840-1250 CE) compared to the Holocene average values (0.015 vs 0.029 cm a<sup>-1</sup>).  
This period, coinciding with the Little Ice Age, is therefore expected to show increased  
background shard concentrations and multi-modal data from 1-cm-resolution samples as each  
centimetre represents ~67 years of accumulation compared to ~25-40 years as seen here over  
520 the Holocene. A higher resolution record for this time period may help to address some of the  
issues detailed here.

For Mt. Churchill there is published evidence for an eruption in the last 500 years: the  
Lena tephra is dated to 310-285 cal yr BP (Payne et al., 2008). It forms a visible bed in  
Yukon Territory (Preece et al., 2014) where it sits on top of ~10 cm of peat accumulation  
525 above the WRAe. It is possible that shards from CL-0 and -2 relate to these events, although  
their age is younger than expected. There has not been any observed modern eruptive activity  
at Mt. Churchill.

There is published evidence for proximal activity at Aniakchak between 560 to 70 yr  
BP (Neal et al., 2001), but only a small proportion of the associated whole rock geochemical  
530 data have a rhyodacitic composition similar to the mid-Holocene CFE II eruption (Bacon et  
al., 2014). Distal tephra preserved in sediment from lakes in the Akhlun Mountains,  
southwest Alaska, however, have similar glass geochemistry and have been dated at around  
400 yr BP (Kaufman et al., 2012). As our age model places the Cascade Lake samples  
between 350-100 cal yr BP, this currently precludes correlation with these known events.  
535 This age range is associated with a relatively high uncertainty due to decreased sedimentation  
rates, so it is possible the chronology does not negate these correlations, but an alternative  
correlation with a younger eruption from Aniakchak (that has not yet been identified distally)  
cannot be ruled out. The large number of analyses that geochemically correlate with  
Aniakchak (47, including 4 dacitic points) over four samples (CL-0, 2, 4 and 7) are therefore  
540 interpreted here as representing as at least one eruptive event from Aniakchak in the last ~400  
years.





## 5.2 Cascade Lake age models

It is not uncommon for ages produced by multiple chronometers to diverge over part or all of a sediment sequence. Individual chronometers have their own inherent strengths and weaknesses, and their different physical properties can be affected by a number of different processes, which in turn affect the preserved and eventually measured signal (e.g. Davies et al., 2018). This is somewhat disheartening as using multiple techniques should provide a check for bias and inaccurate data, but additional independent data can be used to reconcile observed offsets, as shown here.

Once any obvious outliers have been addressed (i.e. steps one and two from Sect. 2.4), it is not always easy to resolve any remaining disagreements between chronometers. For example, from 303-175 cm in Cascade Lake cores there is a divergence between PSV-1 tie-points from geomagnetic field models, from Burial Lake and  $^{14}\text{C}$  ages. Logically, the geomagnetic field models incorporate data from multiple regional palaeomagnetic records, which should give a valuable, albeit spatially smoothed, resulting record for the area. Their reliability at any given coordinate, however, will depend on the amount and quality of data that is in close proximity. A single, nearby well-dated PSV record (here, Burial Lake) could arguably be more relevant than a field model that incorporates multiple datasets. The use of terrestrial macrofossils for radiocarbon dating at Burial Lake and their consistency over the sedimentary sequence suggests they are not affected by, for example, old carbon effects. But, if accurate, the Burial Lake tie-point ages are up to 2000 years older than the other methods for the same composite depths. Outlier analysis performed within OxCal v4.4 was used to assess the ages and statistically identify remaining outliers here (two  $^{14}\text{C}$  ages and three Burial Lake PSV tie-points) in order to resolve this divergence.

The combination of all three chronometers using Bayesian modelling techniques is therefore shown to result in a refined dataset that produces a reliable age model for the past ~21 ka. This demonstrates the importance of independent chronological validation from marker horizons – here, Late Holocene cryptotephra, which provide additional data in a key period – and the power of Bayesian statistics for age modelling. Furthermore, the identification of periods of offset and anomalous or biased ages can allow further investigation of the potential causes, such as mechanical (e.g. mobilisation or redeposition) or chemical (e.g. alteration or degradation) processes affecting the analysed sample material.



Data from Cascade Lake show that PSV-1 provides reliable and accurate tie-points in the Late Holocene that are in agreement with four cryptotephra correlated ages. Comparison  
575 of these data across the whole core shows that at least six  $^{14}\text{C}$  ages are too old, including two initially identified as out of sequence (likely old carbon contamination). However, while the ‘best ages’ produced by PSV-1 are in good agreement with the final age-depth model, the associated uncertainty produced by the geomagnetic field models ( $\pm 500$  years) is broad compared to other methods that can be applied to this time period.

580 The more commonly applied method of  $^{14}\text{C}$  dating can have lower associated errors but is restricted at some Arctic sites by a lack of suitable material. Where macrofossils are available, they may be affected by old carbon contamination or the redeposition of older material. Cascade Lake’s location in limestone terrain likely resulted in a hard-water effect, shown by the  $^{14}\text{C}$  ages reported here. Only four of the eleven analysed samples were included  
585 in the final age-depth model and the identified outliers were variably 500-5000 years too old compared to median modelled ages. As mentioned in other studies the use of either terrestrial material or the humic fraction of sediment is recommended, especially when in limestone terrane (Lowe and Walker, 2000). Nonetheless, this study demonstrates that using multiple independent chronometers with Bayesian age modelling techniques can produce accurate and  
590 reliable age-depth models for Arctic lake sediments.

## 6 Conclusions

This research demonstrates the potential for dating Arctic lake sediments in Alaska using PSV tie-points and cryptotephra correlations. The advantages of tephrochronology include the longer period of time over which it can be applied, the level of precision  
595 associated with known tephra ages and their potential for independently validating other chronometers. We suggest here that the most robust age models can be produced by using a combination of chronostratigraphic techniques in a Bayesian statistical model. While cryptotephra are best defined regionally for the Late Holocene, it is possible that other well-dated cryptotephra from Alaska (e.g. the Early Holocene caldera forming eruptions from  
600 Fisher, Stelling et al., 2005; the late Pleistocene Tephra D, Davies et al., 2016) and ultra-distal sources (e.g. Kamchatka, Japan) could be identified in northern regions.



## Data availability

The major element geochemistry data and associated metadata for individual tephra grains will be made available publicly through the Alaska Volcano Observatory Geochemical Database (Cameron et al., 2019; <http://avo.alaska.edu/geochem>), part of the larger Geologic Database of Information on Volcanoes in Alaska (GeoDIVA). The Bayesian age-depth model generated in this study, including the underlying radiocarbon ages, lead ages and palaeomagnetic secular variation data are available as supplements to both this paper and Steen et al. (this volume).

## 610 Supplement information

**File S1:** OxCal age-depth model input.

**Figure S1:** Bayesian Tau\_Boundary probability density function plots derived using OxCal v4.4 and IntCal20 for the age of Aniakchak CFE II tephra with: all  $^{14}\text{C}$  dates are included (grey right-hand distribution); two  $^{14}\text{C}$  dates removed (green central distribution); and all but two  $^{14}\text{C}$  dates and the NGRIP ice core chronology age (Pearce et al., 2017) (blue left-hand bar). See Table S4 for the ages used for this model.

**Figure S2:** Bayesian Tau\_Boundary probability density function plots derived using OxCal v4.4 and IntCal20 for the age of OP tephra, Opala, Kamchatka. See Table S4 for the ages used for this model.

**Figure S3:** Major element glass geochemical biplots showing wt.%  $\text{SiO}_2$  vs  $\text{K}_2\text{O}$  and  $\text{FeO}$  vs  $\text{CaO}$  for samples with multiple geochemical populations. (a) CL-0 and CL-2; (b) CL-4 and CL-7; (c) CL-31 and CL-61; (d) CL-0, -2, -4 and -7 plotted both by sample and by geochemical correlation with a source volcano or region.

**Figure S4:** OxCal age-depth plot output for the initial Bayesian model for Cascade Lake (v1). Students'-t outlier analysis results are shown. Four ages have more than 50% chance of being an outlier. BL-284 is also excluded as it has an outlier posterior value of 49 and it fails the  $\chi^2$  when combined with pfm9k1b-284.

**Figure S5:** OxCal age-depth output for the final Bayesian model for Cascade Lake (v2). Five outliers from the previous model (v1) were removed and the students'-t outlier analysis results shown good agreement.

**Table S1:** Single point major element glass geochemical data for Cascade Lake samples and reference material.

**Table S2:** Secondary standard data (ID 3506 and Old Crow) for EPMA glass analyses of Cascade Lake samples and reference material.

**Table S3:** Final OxCal age model output for 0-520 cm of CASC13-4A/2D, Cascade Lake.

**Table S4:** Ages for tephra reviewed within this study, listed by associated tephra.

## Author contribution

LJD carried out the research, helped conceptualise the study, and wrote the manuscript. DSK and BJLJ helped conceptualise and fund the study and revised the manuscript. DSK provided the samples. BJLJ carried out some of the analyses.



## 635 Competing interests

The authors declare that they have no conflict of interest.

## Acknowledgements

Jason Briner, David Fortin and Liz Ceperley helped core Cascade Lake; LacCore staff assisted with the initial core analysis and curation. Flett Research, Ltd. provided the <sup>210</sup>Pb  
640 measurements and the W.M. Keck Carbon Cycle Accelerator Mass Spectrometry Laboratory at UC Irvine provided the <sup>14</sup>C measurements.

## Funding sources

Initial research was funded by a National Science Foundation grant (#1107662, DSK).  
645 Subsequent work at the University of Alberta was funded by the Natural Sciences and Engineering Research Council of Canada Discovery Grant and Accelerator Grant (NSERC Discovery grant: #RGPIN-2018-04926; Accelerator: #RGPAS-2018-52250; both BJLJ).

## References

- Abbott, M. B. and Stafford, T. W.: Radiocarbon Geochemistry of Modern and Ancient Arctic Lake Systems, Baffin Island, Canada, *Quat. Res.*, 45(3), 300–311, doi:10.1006/qres.1996.0031, 1996.
- 650 Adolphi, F. and Muscheler, R.: Synchronizing the Greenland ice core and radiocarbon timescales over the Holocene-Bayesian wiggle-matching of cosmogenic radionuclide records, *Clim. Past*, 12(1), 15–30, doi:10.5194/cp-12-15-2016, 2016.
- Ager, T. A.: Late Quaternary vegetation and climate history of the central Bering land bridge from St. Michael  
655 Island, western Alaska, *Quat. Res.*, 60(1), 19–32, doi:10.1016/S0033-5894(03)00068-1, 2003.
- Alaska Volcano Observatory: Alaska Volcano Observatory Online Library, [online] Available from: <https://avo.alaska.edu/volcanoes/index.php>, 2016.
- Andrews, B. J., Dufek, J. and Ponomareva, V.: Eruption dynamics and explosive-effusive transitions during the 1400 cal BP eruption of Opala volcano, Kamchatka, Russia, *J. Volcanol. Geotherm. Res.*, 356, 316–330,  
660 doi:10.1016/j.jvolgeores.2018.02.019, 2018.
- Bacon, C. R., Neal, C. A., Miller, T. P., McGimsey, R. G. and Nye, C. J.: Postglacial eruptive history, geochemistry, and recent seismicity of Aniakchak volcano, Alaska Peninsula., 2014.
- Barletta, F., St-Onge, G., Channell, J. E. T., Rochon, A., Polyak, L. and Darby, D.: High-resolution paleomagnetic secular variation and relative paleointensity records from the western Canadian Arctic:  
665 implication for Holocene stratigraphy and geomagnetic field behaviour, *Can. J. Earth Sci.*, 45(11), 1265–1281,



- doi:10.1139/E08-039, 2008.
- van der Bilt, W. G. M., Lane, C. S. and Bakke, J.: Ultra-distal Kamchatkan ash on Arctic Svalbard: Towards hemispheric cryptotephra correlation, *Quat. Sci. Rev.*, 164, 230–235, doi:10.1016/j.quascirev.2017.04.007, 2017.
- 670 Blaauw, M. and Christen, J. A.: Radiocarbon peat chronologies and environmental change, *J. R. Stat. Soc. Ser. C Appl. Stat.*, 54(4), 805–816, doi:10.1111/j.1467-9876.2005.00516.x, 2005.
- Blackford, J. J., Payne, R. J., Heggen, M. P., de la Riva Caballero, A. and van der Plicht, J.: Age and impacts of the caldera-forming Aniakchak II eruption in western Alaska, *Quat. Res. (United States)*, 82(1), 85–95, doi:10.1016/j.yqres.2014.04.013, 2014.
- 675 Blockley, S. P. E., Pyne-O'Donnell, S. D. F., Lowe, J. J., Matthews, I. P., Stone, A., Pollard, A. M., Turney, C. S. M. and Molyneux, E. G.: A new and less destructive laboratory procedure for the physical separation of distal glass tephra shards from sediments, *Quat. Sci. Rev.*, 24(16–17), 1952–1960, doi:10.1016/j.quascirev.2004.12.008, 2005.
- Blockley, S. P. E., Bronk Ramsey, C. and Pyle, D. M.: Improved age modelling and high-precision age estimates of late Quaternary tephtras, for accurate palaeoclimate reconstruction, *J. Volcanol. Geotherm. Res.*, 177(1), 251–262, doi:10.1016/j.jvolgeores.2007.10.015, 2007.
- 680 Bolton, M., Jensen, B. J. L., Wallace, K. L., Praet, N., Fortin, D., Kaufman, D. S. and De Batist, M.: Machine learning classifiers for attributing tephra to source volcanoes: An evaluation of methods for Alaska tephtras, *J. Quat. Sci.*, In-revisio, n.d.
- 685 Braitseva, O. A., Melekestsev, I. V., Ponomareva, V. V. and Sulerzhitsky, L. D.: Ages of calderas, large explosive craters and active volcanoes in the Kuril-Kamchatka region, Russia, *Bull. Volcanol.*, 57(6), 383–402, doi:10.1007/BF00300984, 1995.
- Braitseva, O. A., Ponomareva, V. V., Sulerzhitsky, L. D., Melekestsev, I. V. and Bailey, J.: Holocene Key-Marker Tephra Layers in Kamchatka, Russia, *Quat. Res.*, 47(2), 125–139, doi:10.1006/qres.1996.1876, 1997.
- 690 Brock, F., Lee, S., Housley, R. A. and Bronk Ramsey, C.: Variation in the radiocarbon age of different fractions of peat: A case study from Ahrenshöft, northern Germany, *Quat. Geochronol.*, 6(6), 550–555, doi:10.1016/j.quageo.2011.08.003, 2011.
- Bronk Ramsey, C.: Deposition models for chronological records, *Quat. Sci. Rev.*, 27(1–2), 42–60, doi:10.1016/j.quascirev.2007.01.019, 2008.
- 695 Bronk Ramsey, C.: Dealing with Outliers and Offsets in Radiocarbon Dating, *Radiocarbon*, 51(3), 1023–1045, doi:10.1017/S0033822200034093, 2009.
- Bronk Ramsey, C.: Recent and Planned Developments of the Program OxCal, *Radiocarbon*, 55(3–4), 720–730, doi:10.2458/azu\_js\_rc.55.16215, 2013.
- Cameron, C. E., Mulliken, K. M., Crass, S. W., Schaefer, J. R. and Wallace, K. L.: Alaska Volcano Observatory geochemical database, version 2., 2019.
- 700 Christen, J. A., Clymo, R. S. and Litton, C. D.: A Bayesian Approach to the Use of  $^{14}\text{C}$  Dates in the Estimation of the Age of Peat, *Radiocarbon*, 37(02), 431–441, doi:10.1017/S0033822200030915, 1995.



- Cook, E., Portnyagin, M., Ponomareva, V., Bazanova, L., Svensson, A. and Garbe-Schönberg, D.: First identification of cryptotephra from the Kamchatka Peninsula in a Greenland ice core: Implications of a widespread marker deposit that links Greenland to the Pacific northwest, *Quat. Sci. Rev.*, 181, 200–206, doi:10.1016/j.quascirev.2017.11.036, 2018.
- 705
- Coulter, S. E., Pilcher, J. R., Plunkett, G., Baillie, M., Hall, V. A., Steffensen, J. P., Vinther, B. M., Clausen, H. B. and Johnsen, S. J.: Holocene tephras highlight complexity of volcanic signals in Greenland ice cores, *J. Geophys. Res. Atmos.*, 117(21), 1–11, doi:10.1029/2012JD017698, 2012.
- 710
- Cox, A.: Latitude Dependence of the Angular Dispersion of the Geomagnetic Field, *Geophys. J. R. Astron. Soc.*, 20(3), 253–269, doi:10.1111/j.1365-246X.1970.tb06069.x, 1970.
- Davies, L. J.: The development of a Holocene cryptotephra framework in northwestern North America, University of Alberta., 2018.
- Davies, L. J., Jensen, B. J. L., Froese, D. G. and Wallace, K. L.: Late Pleistocene and Holocene tephrostratigraphy of interior Alaska and Yukon: Key beds and chronologies over the past 30,000 years, *Quat. Sci. Rev.*, 146, 28–53, doi:10.1016/j.quascirev.2016.05.026, 2016.
- 715
- Davies, L. J., Appleby, P., Jensen, B. J. L., Magnan, G., Mullan-Boudreau, G., Noernberg, T., Shannon, B., Shotyk, W., van Bellen, S., Zaccane, C. and Froese, D. G.: High-resolution age modelling of peat bogs from northern Alberta, Canada, using pre- and post-bomb <sup>14</sup>C, <sup>210</sup>Pb and historical cryptotephra, *Quat. Geochronol.*, 47, 138–162, doi:10.1016/j.quageo.2018.04.008, 2018.
- 720
- Davies, L. J., Jensen, B. J. L. and Locock, A. J.: Do visible Holocene tephra from Mt. Churchill, Alaska, display varying geochemistry across their distributions?, in INQUA XX Congress, Dublin., 2019.
- Davies, S. M.: Cryptotephra: The revolution in correlation and precision dating, *J. Quat. Sci.*, 30(2), 114–130, doi:10.1002/jqs.2766, 2015.
- 725
- Denton, J. S. and Pearce, N. J. G.: Comment on “A synchronized dating of three Greenland ice cores throughout the Holocene” by B. M. Vinther et al.: No Minoan tephra in the 1642 B.C. layer of the GRIP ice core, *J. Geophys. Res. Atmos.*, 113(4), 1–7, doi:10.1029/2007JD008970, 2008.
- Deschamps, C. E., St-Onge, G., Montero-Serrano, J. C. and Polyak, L.: Chronostratigraphy and spatial distribution of magnetic sediments in the Chukchi and Beaufort seas since the last deglaciation, *Boreas*, 47(2), 544–564, doi:10.1111/bor.12296, 2018.
- 730
- Donadini, F., Korte, M. and Constable, C.: Millennial variations of the geomagnetic field: From data recovery to field reconstruction, *Space Sci. Rev.*, 155(1–4), 219–246, doi:10.1007/s11214-010-9662-y, 2010.
- Donovan, J., Kremser, D., Fournelle, J. H. and Goemann, K.: Probe for EPMA: Acquisition, automation and analysis. [online] Available from: www.probesoftware.com, 2015.
- 735
- Dorfman, J. M.: A 37,000-year Record of Paleomagnetic and Environmental Magnetic Variability from Burial Lake, Arctic Alaska., Oregon State University., 2013.
- Fierstein, J.: Explosive eruptive record in the Katmai region, Alaska Peninsula: An overview, *Bull. Volcanol.*, 69(5), 469–509, doi:10.1007/s00445-006-0097-y, 2007.
- de Fontaine, C. S., Kaufman, D. S., Scott Anderson, R., Werner, A., Waythomas, C. F. and Brown, T. A.: Late



- 740 Quaternary distal tephra-fall deposits in lacustrine sediments, Kenai Peninsula, Alaska, *Quat. Res.*, 68(1), 64–78, doi:10.1016/j.yqres.2007.03.006, 2007.  
Fortin, D., Praet, N., McKay, N. P., Kaufman, D. S., Jensen, B. J. L., Haeussler, P. J., Buchanan, C. and De Batist, M.: New approach to assessing age uncertainties – The 2300-year varve chronology from Eklutna Lake, Alaska (USA), *Quat. Sci. Rev.*, 203, 90–101, doi:10.1016/j.quascirev.2018.10.018, 2019.
- 745 Gaglioti, B. V., Mann, D. H., Jones, B. M., Pohlman, J. W., Kunz, M. L. and Wooller, M. J.: Radiocarbon age-offsets in an arctic lake reveal the long-term response of permafrost carbon to climate change, *J. Geophys. Res. Biogeosciences*, 119(8), 1630–1651, doi:10.1002/2014JG002688, 2014.  
Global Volcanism Program: *Volcanoes of the World*, v. 4.8.0., , doi:https://doi.org/10.5479/si.GVP.VOTW4-2013, 2013.
- 750 Jensen, B. J. L.: Tephrochronology of middle to late Pleistocene loess in east-central Alaska, University of Alberta, Edmonton, Alberta, Canada, MSc thesis., 2007.  
Jensen, B. J. L., Froese, D. G., Preece, S. J., Westgate, J. A. and Stachel, T.: An extensive middle to late Pleistocene tephrochronologic record from east-central Alaska, *Quat. Sci. Rev.*, 27(3–4), 411–427, doi:10.1016/j.quascirev.2007.10.010, 2008.
- 755 Jensen, B. J. L., Pyne-O'Donnell, S., Plunkett, G., Froese, D. G., Hughes, P. D. M., Sigl, M., McConnell, J. R., Amesbury, M. J., Blackwell, P. G., van den Bogaard, C., Buck, C. E., Charman, D. J., Clague, J. J., Hall, V. A., Koch, J., Mackay, H., Mallon, G., McColl, L. and Pilcher, J. R.: Transatlantic distribution of the Alaskan White River Ash, *Geology*, 42(10), 875–878, doi:10.1130/G35945.1, 2014.  
Jensen, B. J. L., Beaudoin, A. B., Clynne, M. A., Harvey, J. and Vallance, J. W.: A re-examination of the three most prominent Holocene tephra deposits in western Canada: Bridge River, Mount St. Helens Yn and Mazama, *Quat. Int.*, 500, 83–95, doi:10.1016/j.quaint.2019.03.017, 2019.  
Jensen, B. J. L., Davies, L. J., Nolan, C., Pyne-O'Donnell, S. D. F., Monteath, A. J., Ponomareva, V. V., Portnyagin, M. V., Cook, E., Plunkett, G., Booth, R. K., Hughes, P. D. M., Bursik, M., Luo, Y., Cwynar, L. C. and Pearson, D. G.: A latest Pleistocene and Holocene composite tephrostratigraphic framework for paleoenvironmental records for northeastern North America, *Quat. Sci. Rev.*, n.d.
- 760 Karrow, P. F. and Anderson, T. W.: Palynological Study of Lake Sediment Profiles from Southwestern New Brunswick: Discussion, *Can. J. Earth Sci.*, 12(10), 1808–1812, doi:10.1139/e75-161, 1975.  
Kaufman, D. S., Jensen, B. J. L., Reyes, A. V., Schiff, C. J., Froese, D. G. and Pearce, N. J. G.: Late Quaternary tephrostratigraphy, Ahklun Mountains, SW Alaska, *J. Quat. Sci.*, 27(4), 344–359, doi:10.1002/jqs.1552, 2012.
- 770 Kaufman, D. S., Axford, Y. L., Henderson, A. C. G., McKay, N. P., Oswald, W. W., Saenger, C., Anderson, R. S., Bailey, H. L., Clegg, B., Gajewski, K., Hu, F. S., Jones, M. C., Massa, C., Routson, C. C., Werner, A., Wooller, M. J. and Yu, Z.: Holocene climate changes in eastern Beringia (NW North America) – A systematic review of multi-proxy evidence, *Quat. Sci. Rev.*, 147, 312–339, doi:10.1016/j.quascirev.2015.10.021, 2016.  
Kennedy, K. E., Froese, D. G., Zazula, G. D. and Lauriol, B.: Last Glacial Maximum age for the northwest Laurentide maximum from the Eagle River spillway and delta complex, northern Yukon, *Quat. Sci. Rev.*, 29(9–10), 1288–1300, doi:10.1016/j.quascirev.2010.02.015, 2010.



- Korte, M., Constable, C., Donadini, F. and Holme, R.: Reconstructing the Holocene geomagnetic field, *Earth Planet. Sci. Lett.*, 312(3–4), 497–505, doi:10.1016/j.epsl.2011.10.031, 2011.
- 780 Kuehn, S. C., Froese, D. G. and Shane, P. A. R.: The INTAV intercomparison of electron-beam microanalysis of glass by tephrochronology laboratories: Results and recommendations, *Quat. Int.*, 246(1–2), 19–47, doi:10.1016/j.quaint.2011.08.022, 2011.
- Kyle, P. R., Ponomareva, V. V. and Rourke Schlupe, R.: Geochemical characterization of marker tephra layers from major Holocene eruptions, Kamchatka Peninsula, Russia, *Int. Geol. Rev.*, 53(9), 1059–1097, doi:10.1080/00206810903442162, 2011.
- 785 Lakeman, T. R., Clague, J. J., Menounos, B., Osborn, G. D., Jensen, B. J. L. and Froese, D. G.: Holocene tephra in lake cores from northern British Columbia, Canada, *Can. J. Earth Sci.*, 45(8), 935–947, doi:10.1139/E08-035, 2008.
- Lerbekmo, J. F.: The White River Ash: largest Holocene Plinian tephra, *Can. J. Earth Sci.*, 45(6), 693–700, doi:10.1139/E08-023, 2008.
- 790 Litton, C. D. and Buck, C. E.: The Bayesian Approach To the Interpretation of Archaeological Data, *Archaeometry*, 37(1), 1–24, doi:10.1111/j.1475-4754.1995.tb00723.x, 1995.
- Lowe, D. J., Pearce, N. J. G., Jorgensen, M. A., Kuehn, S. C., Tryon, C. A. and Hayward, C. L.: Correlating tephra and cryptotephra using glass compositional analyses and numerical and statistical methods: Review and evaluation, *Quat. Sci. Rev.*, 175, 1–44, doi:10.1016/j.quascirev.2017.08.003, 2017.
- 795 Lowe, J. J. and Walker, M. J. C.: Radiocarbon Dating the Last Glacial-Interglacial Transition (Ca. 14–9 14 C Ka Bp) in Terrestrial and Marine Records: The Need for New Quality Assurance Protocols, *Radiocarbon*, 42(1), 53–68, doi:10.1017/s0033822200053054, 2000.
- Lund, S., Keigwin, L. and Darby, D.: Character of Holocene paleomagnetic secular variation in the tangent cylinder: Evidence from the Chukchi Sea, *Phys. Earth Planet. Inter.*, 256, 49–58, doi:10.1016/j.pepi.2016.03.005, 2016.
- 800 Mackay, H., Hughes, P. D. M., Jensen, B. J. L., Langdon, P. G., Pyne-O'Donnell, S. D. F., Plunkett, G., Froese, D. G., Coulter, S. E. and Gardner, J. E.: A mid to late Holocene cryptotephra framework from eastern North America, *Quat. Sci. Rev.*, 132, 101–113, doi:10.1016/j.quascirev.2015.11.011, 2016.
- McAneney, J. and Baillie, M.: Absolute tree-ring dates for the Late Bronze Age eruptions of Aniakhchak and 805 Thera in light of a proposed revision of ice-core chronologies, *Antiquity*, 93(367), 99–112, doi:10.15184/aqy.2018.165, 2019.
- Melekestsev, I. V., Felitsyn, S. B. and Kiryanov, V. Y.: The eruption of Opala in A.D. 500 - the largest explosive eruption in Kamchatka in the Christian era., *J. Volcanol. Seismol.*, 13, 21–36, 1992.
- Miller, T. P., McGimsey, R. G., Richter, D. H., Riehle, J. R., Nye, G. J., Yount, M. E. and Dumoulin, J. A.: 810 Catalog of the historically active volcanoes of Alaska, U.S. Dept. of the Interior, U.S. Geological Survey., 1998.
- Monteath, A. J., van Hardenbroek, M., Davies, L. J., Froese, D. G., Langdon, P. G., Xu, X. and Edwards, M. E.: Chronology and glass chemistry of tephra and cryptotephra horizons from lake sediments in northern Alaska, USA, *Quat. Res.*, 88(02), 169–178, doi:10.1017/qua.2017.38, 2017.





- Moore, T. C., Rea, D. K. and Godsey, H.: Regional variation in modern radiocarbon ages and the hard-water  
815 effects in Lakes Michigan and Huron, *J. Paleolimnol.*, 20(4), 347–351, doi:10.1023/A:1007920723163, 1998.
- Neal, C. A., McGimsey, R. G., Miller, T. P., Riehle, J. R. and Waythomas, C. F.: Preliminary Volcano-Hazard  
Assessment for Aniakchak Volcano, Alaska, USGS Open-File Rep., 00–519, 1–35, 2001.
- Nelson, R. E., Carter, L. D. and Robinson, S. W.: Anomalous Radiocarbon Ages from a Holocene Detrital  
Organic Lens in Alaska and their Implications for Radiocarbon Dating and Paleoenvironmental Reconstructions  
820 in the Arctic, *Quat. Res.*, 29(1), 66–71, doi:10.1016/0033-5894(88)90072-5, 1988.
- Nielsen, C. H. and Sigurdsson, H.: Quantitative methods for electron microprobe analysis of sodium in natural  
and synthetic glasses., *Am. Mineral.*, 66(5–6), 547–552, 1981.
- Nilsson, A., Holme, R., Korte, M., Suttie, N. and Hill, M.: Reconstructing Holocene geomagnetic field  
variation: new methods, models and implications, *Geophys. J. Int.*, 198(1), 229–248, doi:10.1093/gji/ggu120,  
825 2014.
- Ólafsdóttir, S., Geirsdóttir, Á., Miller, G. H., Stoner, J. S. and Channell, J. E. T.: Synchronizing holocene  
lacustrine and marine sediment records using paleomagnetic secular variation, *Geology*, 41(5), 535–538,  
doi:10.1130/G33946.1, 2013.
- Oldfield, F., Thompson, R., Crooks, P. R. J., Gedye, S. J., Hall, V. A., Harkness, D. D., Housley, R. a.,  
830 McCormac, F. G., Newton, A. J., Pilcher, J. R., Renberg, I. and Richardson, N.: Radiocarbon dating of a recent  
high latitude peat profile: Stor Åmyran, northern Sweden, *The Holocene*, 7(3), 283–290,  
doi:10.1177/095968369700700304, 1997.
- Olsson, I. U.: Some problems in connection with the evaluation of C 14 dates, *Geol. Föreningen i Stock.  
Förhandlingar*, 96(4), 311–320, doi:10.1080/11035897409454285, 1974.
- 835 Oswald, W. W., Anderson, P. M., Brown, T. A., Brubaker, L. B., Hu, F. S., Lozhkin, A. V., Tinner, W. and  
Kaltenrieder, P.: Effects of sample mass and macrofossil type on radiocarbon dating of arctic and boreal lake  
sediments, *The Holocene*, 15(5), 758–767, doi:10.1191/0959683605hl849rr, 2005.
- Payne, R. J., Blackford, J. and van der Plicht, J.: Using cryptotephra to extend regional tephrochronologies: An  
example from southeast Alaska and implications for hazard assessment, *Quat. Res.*, 69(1), 42–55,  
840 doi:10.1016/j.yqres.2007.10.007, 2008.
- Pearce, C., Varhelyi, A., Wastegård, S., Muschitiello, F., Barrientos, N., O’Regan, M., Cronin, T. M., Gemery,  
L., Semiletov, I., Backman, J. and Jakobsson, M.: The 3.6ka Aniakchak tephra in the Arctic Ocean: A constraint  
on the Holocene radiocarbon reservoir age in the Chukchi Sea, *Clim. Past*, 13(4), 303–316, doi:10.5194/cp-13-  
303-2017, 2017.
- 845 Pearce, N. J. G., Westgate, J. A., Preece, S. J., Eastwood, W. J. and Perkins, W. T.: Identification of Aniakchak  
(Alaska) tephra in Greenland ice core challenges the 1645 BC date for Minoan eruption of Santorini,  
*Geochemistry, Geophys. Geosystems*, 5(3), doi:10.1029/2003GC000672, 2004.
- Pilcher, J. R., Hall, V. A. and McCormac, F. G.: Dates of Holocene Icelandic volcanic eruptions from tephra  
layers in Irish peats, *The Holocene*, 5(1), 103–110, doi:10.1177/095968369500500111, 1995.
- 850 Plunkett, G.: Tephra-linked peat humification records from Irish ombrotrophic bogs question nature of solar



- forcing at 850 cal. yr BC, *J. Quat. Sci.*, 21(1), 9–16, doi:10.1002/jqs.951, 2006.
- Plunkett, G., Coulter, S. E., Ponomareva, V. V., Blaauw, M., Klimaschewski, A. and Hammarlund, D.: Distal tephrochronology in volcanic regions: Challenges and insights from Kamchatkan lake sediments, *Glob. Planet. Change*, 134, 26–40, doi:10.1016/j.gloplacha.2015.04.006, 2015.
- 855 Ponomareva, V., Portnyagin, M., Pendea, I. F., Zelenin, E., Bourgeois, J., Pinegina, T. and Kozhurin, A.: A full holocene tephrochronology for the Kamchatsky Peninsula region: Applications from Kamchatka to North America, *Quat. Sci. Rev.*, 168, 101–122, doi:10.1016/j.quascirev.2017.04.031, 2017.
- Ponomareva, V., Polyak, L., Portnyagin, M., Abbott, P. M., Zelenin, E., Vakhrameeva, P. and Garbe-Schönberg, D.: Holocene tephra from the Chukchi-Alaskan margin, Arctic Ocean: Implications for sediment  
860 chronostratigraphy and volcanic history, *Quat. Geochronol.*, 45(November 2017), 85–97, doi:10.1016/j.quageo.2017.11.001, 2018.
- Portnyagin, M. V., Ponomareva, V. V., Zelenin, E. A., Bazanova, L. I., Pevzner, M. M., Plechova, A. A., Rogozin, A. N. and Garbe-Schönberg, D.: TephraKam: Geochemical database of glass compositions in tephra and welded tuffs from the Kamchatka volcanic arc (northwestern Pacific), *Earth Syst. Sci. Data*, 12(1), 469–  
865 486, doi:10.5194/essd-12-469-2020, 2020.
- Preece, S. J., McGimsey, R. G., Westgate, J. A., Pearce, N. J. G., Hart, W. K. and Perkins, W. T.: Chemical complexity and source of the White River Ash, Alaska and Yukon, *Geosphere*, 10(5), 1020–1042, doi:10.1130/GES00953.1, 2014.
- Pyne-O'Donnell, S. D. F., Hughes, P. D. M., Froese, D. G., Jensen, B. J. L., Kuehn, S. C., Mallon, G.,  
870 Amesbury, M. J., Charman, D. J., Daley, T. J., Loader, N. J., Mauquoy, D., Street-Perrott, F. A. and Woodman-Ralph, J.: High-precision ultra-distal Holocene tephrochronology in North America, *Quat. Sci. Rev.*, 52, 6–11, doi:10.1016/j.quascirev.2012.07.024, 2012.
- Reuther, J., Potter, B., Coffman, S., Smith, H. and Bigelow, N.: Revisiting the Timing of the Northern Lobe of the White River Ash Volcanic Event in Eastern Alaska and Western Yukon, *Radiocarbon*, 62(1), 169–188,  
875 doi:10.1017/RDC.2019.110, 2020.
- Riehle, J. R., Meyer, C. E., Ager, T. A., Kaufman, D. S. and Ackerman, R. E.: The Aniakchak tephra deposit, a Late Holocene marker horizon in western Alaska., 1987.
- Schoning, K., Charman, D. J. and Wastegård, S.: Reconstructed water tables from two ombrotrophic mires in eastern central Sweden compared with instrumental meteorological data, *The Holocene*, 15(1), 111–118,  
880 doi:10.1191/0959683605h1772rp, 2005.
- Schuur, E. A. G., Bockheim, J., Canadell, J. G., Euskirchen, E., Field, C. B., Goryachkin, S. V., Hagemann, S., Kuhry, P., Lafleur, P. M., Lee, H., Mazhitova, G., Nelson, F. E., Rinke, A., Romanovsky, V. E., Shiklomanov, N., Tarnocai, C., Venevsky, S., Vogel, J. G. and Zimov, S. A.: Vulnerability of Permafrost Carbon to Climate Change: Implications for the Global Carbon Cycle, *Bioscience*, 58(8), 701–714, doi:10.1641/B580807, 2008.
- 885 Steen, D. P., Stoner, J. S., Kaufman, D. S. and Briner, J. P.: 21,000 years of paleomagnetic secular variation and relative paleointensity at Cascade Lake, north-central Brooks Range, Arctic Alaska: Assessing offsets between PSV and radiocarbon-based age models (submitted), *Geochronology*, n.d.



- Stelling, P., Gardner, J. E. and Begét, J.: Eruptive history of Fisher Caldera, Alaska, USA, *J. Volcanol. Geotherm. Res.*, 139(3–4), 163–183, doi:10.1016/j.jvolgeores.2004.08.006, 2005.
- 890 Stoner, J. S., Channell, J. E. T., Mazaud, A., Strano, S. E. and Xuan, C.: The influence of high-latitude flux lobes on the Holocene paleomagnetic record of IODP Site U1305 and the northern North Atlantic, *Geochemistry, Geophys. Geosystems*, 14(10), 4623–4646, doi:10.1002/ggge.20272, 2013.
- Swindles, G. T., De Vleeschouwer, F. and Plunkett, G.: Dating peat profiles using tephra: stratigraphy, geochemistry and chronology, *Mires Peat*, 7, 1–9, 2010.
- 895 Turney, C. S. M., Coope, G. R., Harkness, D. D., Lowe, J. J. and Walker, M. J. C.: Implications for the Dating of Wisconsinan (Weichselian) Late-Glacial Events of Systematic Radiocarbon Age Differences between Terrestrial Plant Macrofossils from a Site in SW Ireland, *Quat. Res.*, 53(1), 114–121, doi:10.1006/qres.1999.2087, 2000.
- Tylmann, W., Bonk, A., Goslar, T., Wulf, S. and Grosjean, M.: Calibrating 210Pb dating results with varve  
900 chronology and independent chronostratigraphic markers: Problems and implications, *Quat. Geochronol.*, 32, 1–10, doi:10.1016/j.quageo.2015.11.004, 2016.
- Vinther, B. M., Clausen, H. B., Johnsen, S. J., Rasmussen, S. O., Andersen, K. K., Buchardt, S. L., Dahl-Jensen, D., Seierstad, I. K., Siggaard-Andersen, M. L., Steffensen, J. P., Svensson, A., Olsen, J. and Heinemeier, J.: A synchronized dating of three Greenland ice cores throughout the Holocene, *J. Geophys. Res. Atmos.*, 111(13),  
905 doi:10.1029/2005JD006921, 2006.
- Waitt, R. B. and Begét, J. E.: Volcanic processes and geology of augustine volcano, Alaska, *US Geol. Surv. Prof. Pap.*, (1762), 1–78 [online] Available from: <http://www.scopus.com/inward/record.url?eid=2-s2.0-80053057972&partnerID=tZOtx3y1>, 2009.
- Watson, E. J., Swindles, G. T., Lawson, I. T. and Savov, I.: Spatial variability of tephra and carbon  
910 accumulation in a Holocene peatland, *Quat. Sci. Rev.*, 124, 248–264, doi:10.1016/j.quascirev.2015.07.025, 2015.
- Zander, P. D., Kaufman, D. S., McKay, N. P., Kuehn, S. C. and Henderson, A. C. G.: Quaternary  
Geochronology Using correlated tephra to refine radiocarbon-based age models, upper and lower Whitshed  
Lakes, south-central Alaska, *Quat. Geochronol.*, 45(October 2017), 9–22, doi:10.1016/j.quageo.2018.01.005,  
915 2018.
- Zoltai, S. C.: Late Quaternary volcanic ash in the peatlands of central Alberta, *Can. J. Earth Sci.*, 26(2), 207–214, doi:10.1139/e89-017, 1989.